Serb. Astron. J. № 162 (2000), 7 – 33 **UDC 52–355.3/524.7–82**
Original scientific paper

THE H_β LINE SHAPE OF Akn 120

N. Stanić, L. Č. Popović, A. Kubičela and E. Bon

Astronomical Observatory, Volgina 7, 11160 Belgrade-74, Yugoslavia

(Received: December 19, 2000)

SUMMARY: We present here the Akn 120 H_β line profiles from 97 spectra observed from 1977 till 1990 at Crimean Astrophysical Observatory (Appendix 1). The H_β line has been fitted with three broad and one narrow Gaussian throughout the whole considered period. The central broad components of the H_β and a shelf cause the H_β line shape variation. Three broad Gaussians may suggest the existence of three broad line regions in the central part of the Akn 120. Long-term H_β line shape variations in spectra of this galaxy are discussed.

1. INTRODUCTION

Emission line profiles of Active Galactic Nuclei (AGNs) usually show variabilities. Investigations of these variations could provide information about the structure, size and kinematics of the emitting gas in central part of these objects (see, e.g., Foltz *et al.* 1983, Peterson *et al.* 1985, 1989, 1998, Peterson and Gaskell 1991, Peterson 1993, Ernens *et al.* 1995, Winge *et al.* 1996, etc.). According to the standard model, the broad emission lines observed in spectra of AGNs originate in the high-velocity gas of the surrounding Broad Line Regions (BLR) ionized by the UV and optical continuum radiation of a compact central source. Fluctuation in the ionizing continuum causes the variations in emission line fluxes. Also, the structure of the BLR may be investigated through the analyses of the broad emission line profiles.

One of the Sy1 galaxies which has a large-amplitude variability in continuum and in spectral line shapes is the Akn 120 (Peterson *et al.* 1985, 1989, 1998, Peterson and Cota 1987, Korista 1992, Winge *et al.* 1996, Popović *et al.* 2001). The galaxy was monitored several times (see e.g. Peterson *et al.* 1998). These investigations show that the integrated flux in the broad emission lines changes very rapidly (Peterson *et al.* 1989, Winge *et al.* 1996) and that this region is very small (Peterson *et al.* 1998).

The analyses of emission line shapes of the Akn 120 have shown that Balmer lines are complex in structure and variable (Korista 1992). The decomposition of H_β and other broad lines indicates a stratification in the BLR (Korista 1992). The complex and strong profile variations of broad lines of Akn 120 indicate very dynamic processes in the emitting gas.

Here we analyse the H_β line profile of Akn 120 from a set of 97 spectra observed at Crimean Astrophysical Observatory (CrAO) in the period from 1971 till 1990. In order to reveal the structure of the emitting region of Akn 120 we have decomposed the broad H_β line into several gausian components.

Table 1. Temporal-distribution and number of the observed spectra (in Heliocentric Julian Days – HJD.)

group	1	2	3	4	5	6	7	8	9	10
from HJD 2440000 +	3435	3790	4173	4522	4881	5263	5619	5997	6853	7832
till HJD 2440000 +	3574	3934	4289	4672	5054	5412	5734	6088	7124	7944
mean HJD 2440000 +	3494	3879	4229	4577	4958	5331	5695	6058	7014	7888
numbers of spectra	14	14	9	5	15	12	11	6	6	4

2. THE OBSERVATIONS AND PROCEDURE OF REDUCTION

The present observational material contains 97 spectra in the wavelength interval 4500-5300 *Å* obtained by K. K. Chuvaev on 2.6 m Shain telescope at CrAO during the period 1977-1990 (from HJD 2443435 till 2447944).

All spectra were scanned on two-coordinate CrAO microphotometer. The further treatment, including all instrumental and sky background corrections were carried out at CrAO too (Doroshenko *et al.* 1999). The wavelength and flux calibration were made using the SPE data reduction package developed by S. G. Sergeev. The wavelength calibration was based on the night sky lines and narrow emission lines of the galaxy. The redshift of Akn 120 is accepted equal to z=0.03248 (Foltz *et al.* 1983).

All the 97 H_β spectra are shown in Appendix I. Table 2 presents their main observational data.

Taking into account the temporal distribution of the observations (big seasonal gaps) the spectra have been divided into 10 groups, Table 1.

The spectra within groups have been averaged. In the mean spectra noises and some short-term variations are to some extent suppressed and possible long-lasting-features better expressed. The local continuum in four narrow zones around 4500, 4900, 5270 and 5630 *Å* was interpolated with a second-degree polynomial and subtracted from the observed spectra.

The mean spectra have been normalized to the O III 5007 narrow emission line flux spectral density. It was found as the height of the emission line peak above a straight line connecting the two bottoms of the O III 5007 emission line wings (supposedly above the common H_β + Fe II shelf profile). Hereafter this photometric quantity is simply refered to as relative intensity. To the relative unit defined in this way, an absolute measure might correspond: for example, 7 $\times$ 10^{-15} erg cm^{-2} s^{-1} Å^{-1} given by Kollatschny *et al.* (1981).

One has to notice that narrow O III lines (especially O III 4959) are unusually weak in Akn 120, hence the present flux calibration based on O III line is less reliable than it normally would be.

3. THE SHAPE OF BROAD LINES

In Fig. 1. we present all ten considered profiles and an averaged profile obtained from these considered profiles.

The broad H_β line has two peaks shifted blueward and redward from the line center defined by narrow emission lines. The peak are more or less clearly resolved. Besides, the H_β is blended with O III (4959, 5007) and some other emission lines (Jackson and Brown 1989, Meyers and Peterson 1985, Korista 1992).

The shape of H_β shows very strong variation (Fig. 1), especially in central part of the line. Here one should notice three parts: shoulder in the blue part of profile, a blue and a red peak. The stronger variation is noted in the red peak.

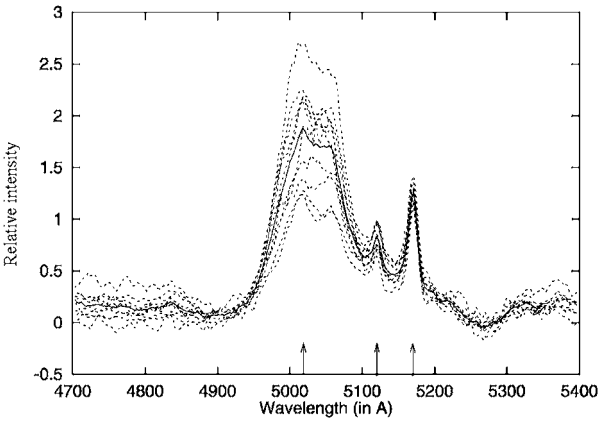

Fig. 1. *The shape of H_β in all considered periods (broken lines) and an averaged profile H_β from these periods (full line). The arrows at the bottom indicate the systemic redshifts of H_β, O III 4959 and O III 5007 lines.*

4. THE GAUSSIAN ANALYSIS

Our approach is to decompose the H_β spectral line profile into a minimum number of Gaussians which would convincingly fit the observed profile.

Then, there might be some justification in a physical interpretation of the obtained Gaussian components.

In order to decrease the number of free parameters, some relations among the fitting Gaussians have been established a priori (Popović and Mediavilla 1997). Namely, the three Gaussians representing two narrow O III lines and a narrow H_β component are preconditioned to have the same systemic redshift, z=0.03248 (Foltz *et al.* 1983), and the intensity ratio of the two O III lines has been supposed to be 1 : 3.03. Also, the ratio of the full widths of these two lines and narrow H_β component are fixed in proportion with their wavelengths as in Popović *et al.* (2001)

$$\frac{W(H_\beta)}{\lambda_{4861}} = \frac{W(OIII_{4959})}{\lambda_{4959}} = \frac{W(OIII_{5007})}{\lambda_{5007}},$$

where W(H_β) is the width of H_β narrow component, W($OIII_4$959) and W($OIII_5$007) are widths of the two O III (4959, 5007) lines.

We obtained the best fit of the averaged H_β wave length region with six Gaussians (Fig. 2) and one shelf component. During the considered period, in all groups, H_β can be resolved into four components. Three of them are broad and similar to one in the case of the averaged profile: the broadest Gaussian covers the other two broad ones which are displaced

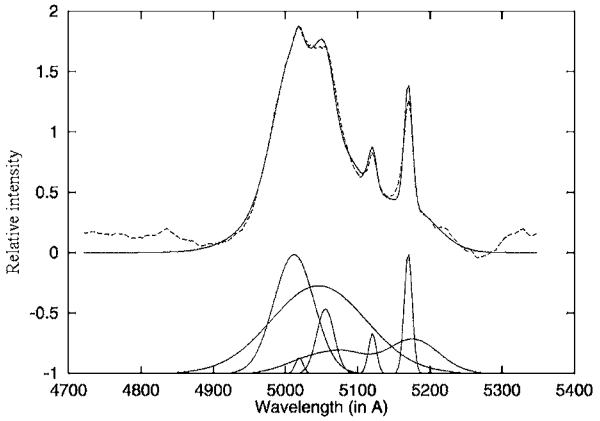

Fig. 2. *Decomposition of the averaged shape of the H_β line. The observed profile is delineated by the dashed lines and the best fit is shown as the full line.*

toward the blue and red side from the central H_β narrow line wavelength.

Besides the four Gaussians closely connected with H_β and the two corresponding O III lines, a wide multipeaked structure (the shelf) can be noticed at the bottom (Fig. 2). The origin of the red shelf in Akn 120 and H_β lines in other AGNs has been discussed in several papers (Foltz et al. 1983, Mayers and Peterson 1985, Stirpe *et al.* 1989, van Groningen and de Bruyn 1989, Korista 1992). The investigations show that two lines from Fe II, multiplet 42, cannot explain the red shelf and common solution is to assume the existence of broad O III lines. Kollatschny *et al.* (1981) investigated the combined UV and optical spectra of Akn 120 and they noticed that UV and optical Fe II emission is very strong. Moreover they found that Akn 120 shows unusually strong Fe II emission in the UV spectra. On the other hand calculations performed by Joly (1988) indicate that multiplets 25 and 36 of Fe II may have large contribution in the red wing of the H_β. That was our reason to accept the red shelf Fe II template which has been proposed by Korista (1992). We have supposed that the red shelf is composed of nine Fe II lines belonging to the multiplets 25, 36 and 42. We took the relative strenght of these lines from Korista (1992) and we supposed that all of the lines originated in the same conditions (in the same region), meaning that all of them should have the same $W/_\lambda$ and shift.

5. RESULTS AND CONCLUSION

The spectra in each of the ten groups from Table I were averaged and decomposed in the same way as it was done with the averaged profile of all the 97 spectra in Fig. 2. These are shown in Figs. 3-12.

We are focused here on the broad H_β components. However, in some groups of spectra a small and narrow Gaussian at $\lambda \approx 5020\AA$ is visible. It has to represent the H_β narrow emission spectral line of Akn 120 which has been found to amount to only eigth percent of the O III 5007 line flux (Korista 1992). In Figs. 3-12, the height of the narrow Gaussian runs from zero (groups 4,5,6 and 8) to the maximum value of about 0.4 (group 10). As this component should be detectable in all of our cases, we estimate the present observational errors to amount to about 0.1-0.2 in relative intensity units.

Figs. 3-12 show that the complex shape of the H_β line of Akn 120 can be decomposed into four components, where three of them are broad. Also, one red shelf composed of nine Fe II lines from multiplets 25, 36 and 42 is present in the red wing of the H_β.

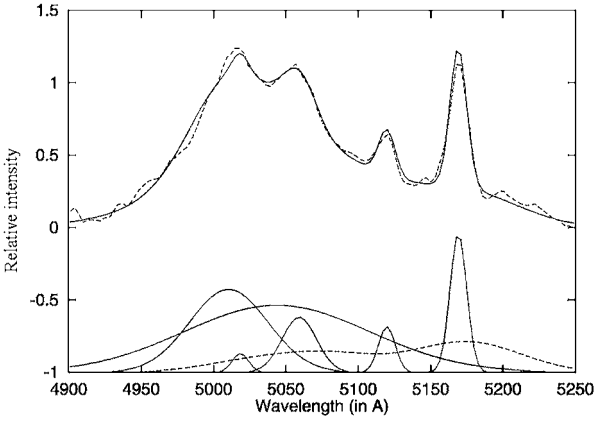

Fig. 3. *The averaged H_β line from group 1, and its decomposition The bottom dashed line represents the FeII shelf.*

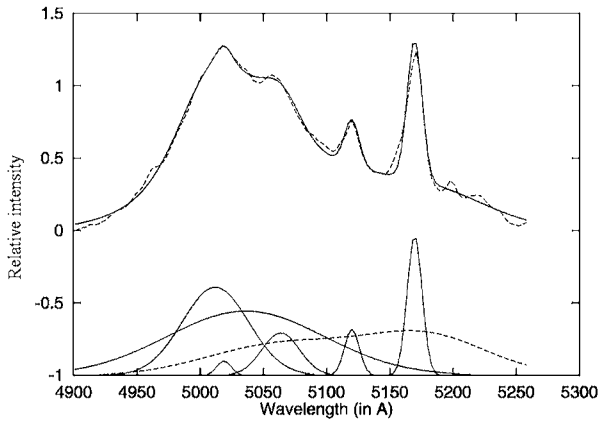

Fig. 4. *The averaged H_β line from group 2, and its decomposition.*

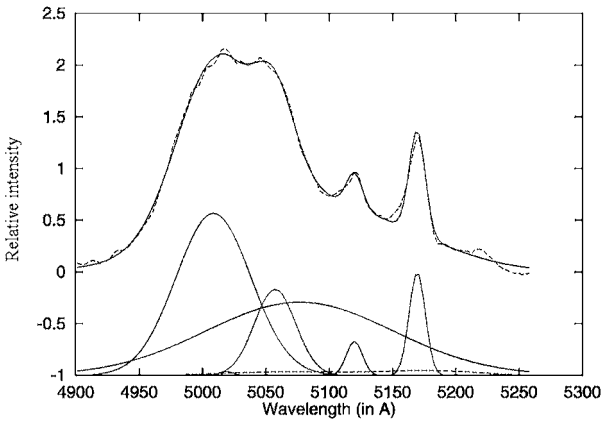

Fig. 7. *The averaged H_β line from group 5, and its decomposition.*

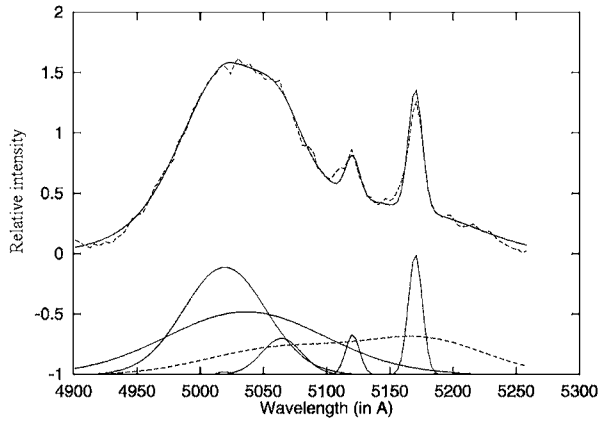

Fig. 5. *The averaged H_β line from group 3, and its decomposition.*

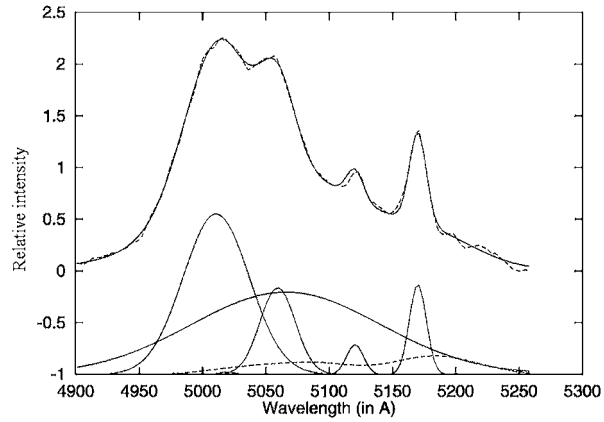

Fig. 8. *The averaged H_β line from group 6, and its decomposition.*

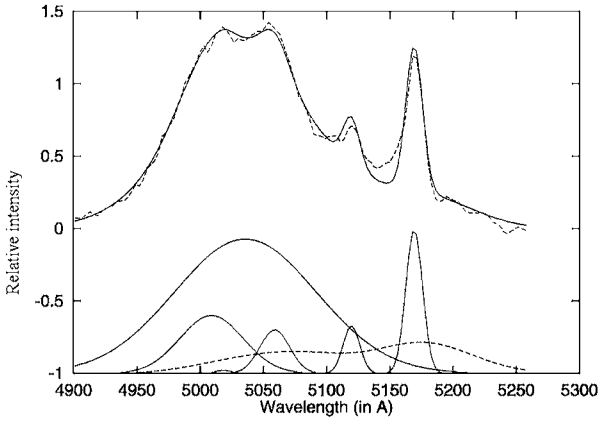

Fig. 6. *The averaged H_β line from group 4, and its decomposition.*

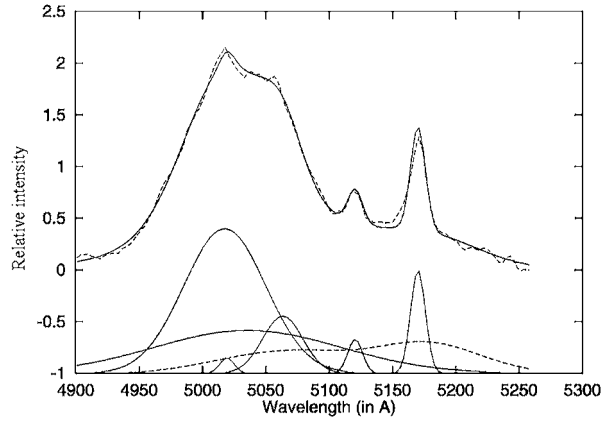

Fig. 9. *The averaged H_β line from group 7, and its decomposition.*

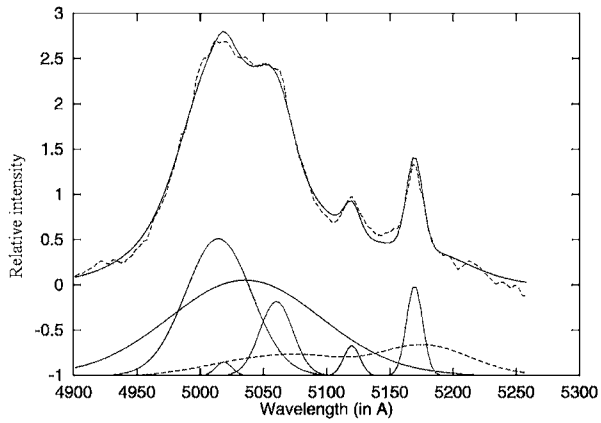

Fig. 10. *The averaged H_β line from group 8, and its decomposition.*

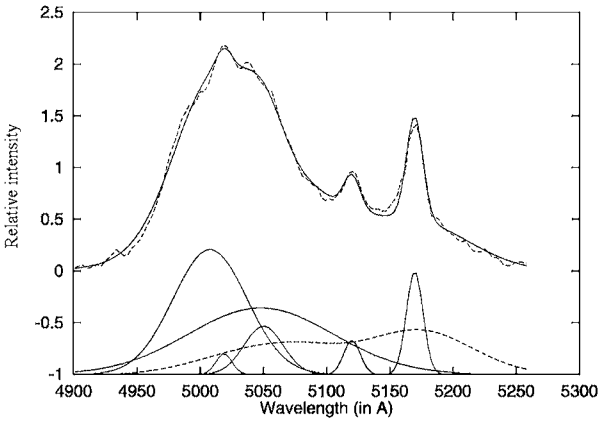

Fig. 11. *The averaged H_β line from group 9, and its decomposition.*

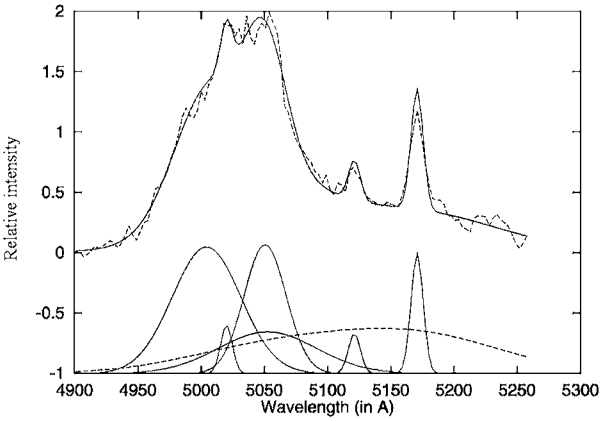

Fig. 12. *The averaged H_β line from group 10, and its decomposition.*

The broadest component has Full With at Half maximum $w \approx 6000 km/s$, whereas the other two broad components have $3000 km/s$ (component shifted toward blue) and $1000 km/s$ (component shifted toward red).

The shape of Akn 120 indicates that we have one very broad line-emitting region and two regions of emitting gas where the systematic emitting gas motions are present. It seems that one of the last two regions has high random velocity of emitters ($W \approx$ 3000 km/s) approaching line-of-sight velocities, and the other has smaller random velocity of emitters (about $1000 km/s$) with receding line-of-sight velocities.

The presence of the three broad Gaussians and their relations in H_β line may indicate the existence of two broad line regions in Akn 120 as it was, in general, suggested by Gaskell (1999).

In particular, we suggest a model, Fig. 13, where the central peaks of H_β emission line profile originate in BLR clouds distributed within a biconical region, BLR1+BLR2, coaxial with the axis of the overall AGN's cylindrical structure (Popović *et al.* 2001). The main contribution to the wings of the H_β line may come from an emitting ring within the accretion disk or from an elipsodial or disk-like region, BLR3, surrounding the AGN's central engine.

Further development of the idea might be based on the replacement of the broadest Gaussian by a disk-hypothesis profile, and the other two broad Gaussians by a profile obtained by assuming a biconical BLR structure.

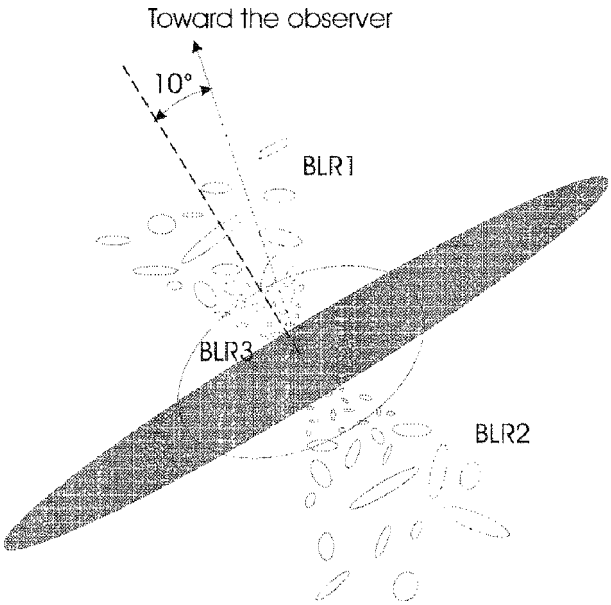

Fig. 13. *Possible location of the two-component BLR in Akn 120. The first component includes two axial subregions, BLR1 and BLR2. The second component, BLR3, may comprise a central part of the accretion disk or an oval volume surrounding the very centre of the AGN (Popović et al. 2001).*

Acknowledgements – This work is a part of the project "Astrometrical, Astrodynamical and Astrophysical investigations", supported by Ministry of Science and Technology of Serbia.

REFERENCES

Doroshenko, V.T., Sergeev, S.G., Pronik, V.I., Chuvaev, K. K.: 1999, *Astron. Lett.* **25**, 569.

Foltz, C.B., Wilkes, B.J. and Peterson, B.M.: 1983, *Astrophys. J.* **88**, 1703.

Gaskell, C.M.: 1983, Proc. 24 Liege Inter. Ap. Colloquium, Univ. de Liege, Liege, 473.

Gaskell, C.M.: 1996, *Astrophys. J. Lett.* **464**, 107.

Gaskell, C.M.: 1999, in Structure and Kinematics of Quasar Broad Line Regions (eds. G. M. Gaskell, V. N. Brandt, M. Dietruch, D. Dultain-Hacyan, M. Eracleous), *ASP Conference Series* **175**, 423.

Jackson, N. and Browne, I.W.A.: 1989, *Mon. Not. Roy. Astron. Soc.* **236**, 97.

Joly, M.: 1988, *Astron. Astrophys.* **192**, 87.

Kollatschny, W., Schleicher, H., Fricke, K.J. and Yorke, H. W.: 1981, *Astron. Astrophys.* **104**, 198.

Korista, K.: 1992, *Astrophys. J. Suppl. Ser.* **79**, 285.

Meyers, K.A.and Peterson, B.M.: 1985, *Publ. Astron. Soc. Pacific*, **97**, 734.

Peterson, B.M., Mayers, K.A., Capriotti, E.R., Foltz, C.B., Wilkes, B.J. and Miller, H.R.: 1985, *Astrophys. J.* **292**, 164.

Peterson, B.M. and Cota, S.A.: 1987, *Astrophys. J.* **94**, 7.

Peterson, B.M., Korista, K.T. and Wagner, R.M.: 1989, *Astrophys. J.* **98**, 500.

Peterson, B.M. and Gaskell, C.M.: 1991, *Astrophys. J.* **368**, 152.

Peterson, B.M.: 1993, *Publ. Astron. Soc. Pacific*, **105**, 247.

Petersonk, B.M., Wanders, I., Bertram R., Hunley J.F.: 1998, *Astrophys. J.* **501**, 82.

Popović, L.Č and Mediavilla E.: 1997, *Publ. Astron. Obs. Belgrade*, **57**, 95.

Popović, L.Č., Trajković, N., Kubičela, A., Doroshenko, V.T., Sergeev, S.G., Bon, E. and Stanić, I.: 1998, Proc. of the Second Yugoslav-Belarussian Symposium on Physics & Diagnostic of Laboratory & Astrophysical Plasmas, 139.

Popović, L.Č., Stanić, N., Kubičela, A., Bon, E: 2001, *Astron. Astrophys.* accepted.

Stirpe, G.M., van Groningen, E. and de Bruyn, A.G.: 1998, *Astron. Astrophys.* **211**, 310.

Stuchlik, Z.: 1998, Proc. 20th Stellar Conference eds. Dushek, J. and Zejda, M. N., Copernicus Obs. And Planetarium, Brno, 418.

van Groningen, E. and de Bruyn, A. G.: 1989, *Astron. Astrophys.* **211**, 293.

Winge, C., Peterson, B.M., Pastoriza, M.G. and Storchi-Bergman, T.: 1996, *Astrophys. J.* **469**, 648.

APPENDIX I

ATLAS OF 97 SPECTRA OF Akn 120

Table 2. Observational parameters of the Akn spectra

The columns contain:
Object – The file names identifying tab individual spectra,
HJD – Heliocentric Julian date of the observation,
Date – The date of observation,
T – UT of the beginning of the exposure,
Exp – Duration of the exposure,
Difr. gr. – Number of grooves per mm on the applied diffractional grating,
Seeing – Seeing quality,
Slit – The width of the spectrograph entrance slit,
z – Zenith distance of the observed object,
Group – Belonging of the spectrum to one of 10 groups of spectra in Table 1.

Object	HJD	Date	T	Exp	Difr. gr.	,Seeing' [arcsec]	Slit [arcsec]	z	Group
	2440000+	yymmdd	hh:mm	min					
Akn00001	3435.562	771018	28:18	12	600	<2	1.20	45.3	1
Akn00004	3437.530	771020	27:29	19	600	6	1.20	46.0	1
Akn00005	3437.544	771020	27:50	18	600	6	1.20	45.5	1
Akn00006	3437.558	771020	28:09	18	600	6	1.20	45.2	1
Akn00009	3486.465	771208	25:52	20	600	5	1.30	47.0	1
Akn00010	3486.482	771208	26:18	18	600	5	1.30	49.5	1
Akn00011	3486.496	771208	26:37	19	600	4	1.30	51.0	1
Akn00015	3489.425	771211	24:50	30	600	6	1.25	45.2	1
Akn00016	3522.407	780113	24:30	20	600	2	1.25	53.0	1
Akn00017	3522.421	780113	24:50	20	600	2	1.25	56.0	1
Akn00019	3525.380	780116	23:57	08	600	3	1.25	50.8	1
Akn00020	3525.389	780116	24:08	14	600	3	1.25	51.5	1
Akn00023	3545.292	780205	21:48	18	600	3	1.25	37.0	1
Akn00030	3574.221	780306	20:08	20	600	2	1.25	47.0	1
Akn00035	3790.583	781008	28:49	13	600	2–3	1.85	44.5	2
Akn00036	3790.592	781008	29:03	13	600	2–3	1.85		2
Akn00040	3814.525	781101	27:22	15	600	2.5	1.85		2
Akn00045	3816.489	781103	26:31	15	600	2.5	1.85	45.5	2
Akn00047	3816.512	781103	27:04	15	600	2.5	1.85	45.3	2
Akn00049	3816.533	781103	27:35	12	600	2.5	1.85	45.0	2
Akn00050	3931.271	790226	21:14	30	600	2	1.85	49.6	2
Akn00052	3932.245	790227	20:44	15	600	2.5	1.85	47.3	2
Akn00054	3932.267	790227	21:16	15	600	<2.5	1.85	49.8	2
Akn00056	3933.209	790228	19:53	15	600	2	1.85	45.0	2
Akn00058	3933.232	790228	20:26	15	600	2.5	1.85		2
Akn00060	3933.255	790228	20:58	15	600	2.5	1.85	49.0	2
Akn00061	3934.236	790301	20:30	18	600	2.5	1.85	46.9	2
Akn00062	3934.249	790301	20:49	18	600	2.5	1.85	48.2	2

Object	HJD	Date	T	Exp	Difr. gr.	,Seeing' [arcsec]	Slit [arcsec]	z	Group
	2440000+	yymmdd	hh:mm	min					
Akn00065	4173.566	791026	28:17	24	600	3–4	1.90	45.5	3
Akn00067	4192.481	791114	26:18	15	600	2–2.5	1.90	44.8	3
Akn00070	4193.507	791115	26:55	16	600	3	1.90	45.5	3
Akn00071	4193.520	791115	27:14	16	600	3	1.90		3
Akn00073	4222.382	791214	23:55	15	600	3	1.89		3
Akn00077	4254.356	800115	23:18	17	600	2–3	1.85		3
Akn00080	4254.393	800115	24:12	15	600	2–3	1.85		3
Akn00081	4289.294	800219	21:54	15	600	2.5	1.85		3
Akn00082	4289.306	800219	22:10	16	600	2.5	1.85		3
Akn00084	4522.539	801009	27:46	14	600	2	1.80	47.0	4
Akn00087	4522.571	801009	28:31	14	600	2	1.80		4
Akn00088	4584.484	801210	26:22	14	600	<2	1.90	50.0	4
Akn00089	4584.494	801210	26:37	14	600	<2	1.90		4
Akn00092	4672.221	810308	20:11	15	600	1.5	1.85		4
Akn00094	4881.568	811003	28:29	12	600	2.0	1.90	45.0	5
Akn00095	4881.578	811003	28:44	12	600	2.0	1.90	45.0	5
Akn00098	4885.564	811007	28:22	14	600	1.5	1.90	45.0	5
Akn00100	4933.436	811124	25:14	14	600	2	1.90	45.0	5
Akn00101	4933.447	811124	25:30	14	600	2	1.90	45.0	5
Akn00104	4934.435	811125	25:11	15	600	2	1.90		5
Akn00107	4934.467	811125	25:58	14	600	2	1.90		5
Akn00108	4961.399	811222	24:18	18	600	2.5–4	1.90		5
Akn00111	4961.461	811222	25:47	18	600	3	1.90		5
Akn00112	4989.310	820119	22:15	12	600	<2	1.60	45.0	5
Akn00113	4989.319	820119	22:28	12	600	<2	1.60		5
Akn00116	4990.373	820120	23:45	14	600	2	1.60	50.0	5
Akn00118	5018.261	820217	21:08	12	600	<2	1.50	46.0	5
Akn00119	5018.272	820217	21:23	13	600	<2	1.50	47.3	5
Akn00122	5054.278	820325	21:33	18	600	3	1.80		5
Akn00123	5263.532	821020	27:31	20	600	<3	1.70	45.6	6
Akn00125	5264.538	821021	27:43	14	600	<2	1.70	45.0	6
Akn00126	5264.549	821021	27:58	14	600	<2	1.70	44.8	6
Akn00128	5324.434	821220	25:07	22	600	2	1.75	47.0	6
Akn00129	5324.467	821220	25:56	18	600	2	1.75	50.8	6
Akn00131	5325.468	821221	25:58	18	600	<2	1.75	51.4	6
Akn00132	5325.481	821221	26:17	16	600	<2	1.75		6
Akn00134	5326.400	821222	24:22	12	600	<2	1.70	45.0	6
Akn00135	5326.410	821222	24:37	12	600	<2	1.70		6
Akn00137	5410.239	830316	20:38	15	600	2	1.75	53.5	6
Akn00138	5410.253	830316	20:58	14	600	2	1.75	56.0	6
Akn00140	5412.267	830318	21:17	17	600	2.5	1.80	59.8	6
Akn00142	5619.560	831011	28:14	17	600	<2	1.80	45.0	7

Object	HJD	Date	T	Exp	Difr. gr.	,Seeing' [arcsec]	Slit [arcsec]	z	Group
	2440000+	yymmdd	hh:mm	min					
Akn00144	5620.507	831012	26:59	14	600	<2	1.80	48.0	7
Akn00146	5674.452	831205	25:38	11	600	2	1.70	45.0	7
Akn00147	5674.461	831205	25:50	12	600	2	1.70		7
Akn00150	5705.382	840105	23:56	14	600	2	1.80	46.0	7
Akn00153	5706.366	840106	23:35	12	600	<2	1.80	45.2	7
Akn00154	5706.377	840106	23:50	12	600	2	1.80		7
Akn00157	5733.337	840202	22:55	12	600	2	1.80	50.0	7
Akn00158	5733.347	840202	23:10	12	600	2	1.80		7
Akn00161	5734.352	840203	23:17	12	600	2	1.80		7
Akn00165	5997.550	841023	28:01	11	120	<2	1.70	45.0	8
Akn00166	5997.558	841023	28:13	10	120	<2	1.70		8
Akn00168	6087.340	850121	22:58	13	600	2–2.5	1.85	46.8	8
Akn00169	6087.352	850121	23:13	16	600	2–2.5	1.85		8
Akn00172	6088.304	850122	22:06	12	600	<2	1.85	45.0	8
Akn00173	6088.313	850122	22:19	12	600	<2	1.85	45.0	8
Akn00174	6410.437	851210	25:17	10	600	<2	1.80	45.0	
Akn00175	6410.446	851210	25:29	10	600	<2	1.80	46.0	
Akn00177	6853.238	870226	20:35	12	600	2.5	1.85		9
Akn00178	6853.247	870226	20:48	12	600	2.5	1.85		9
Akn00180	7091.522	871022	27:20	12	600	<2	1.80	46.0	9
Akn00182	7124.448	871124	25:32	12	600	<2	1.80	45.0	9
Akn00183	7124.457	871124	25:45	12	600	<2	1.80		9
Akn00184	7124.468	871124	26:00	14	600	<2	1.80	45.0	9
Akn00185	7832.502	891101	26:47	20	1200	2.5	1.80	51.0	10
Akn00186	7832.525	891101	27:12	35	1200	2.0	1.80		10
Akn00188	7944.279	900221	21:33	13	600	2.0	1.80		10
Akn00191	7944.303	900221	22:13	04	1200	2.0	1.80		10

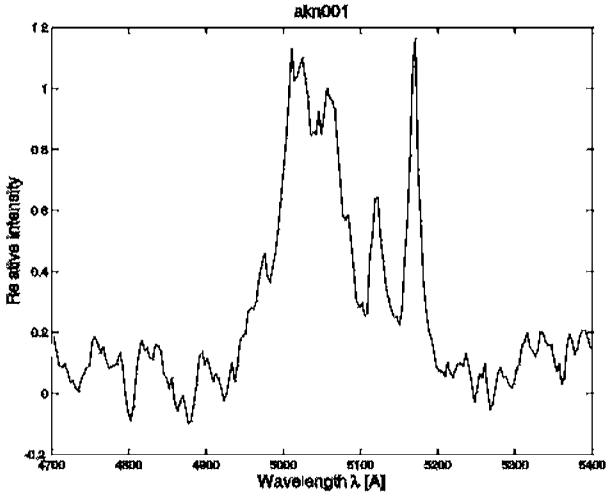
akn001
Relative Intensity
Wavelength λ [A]

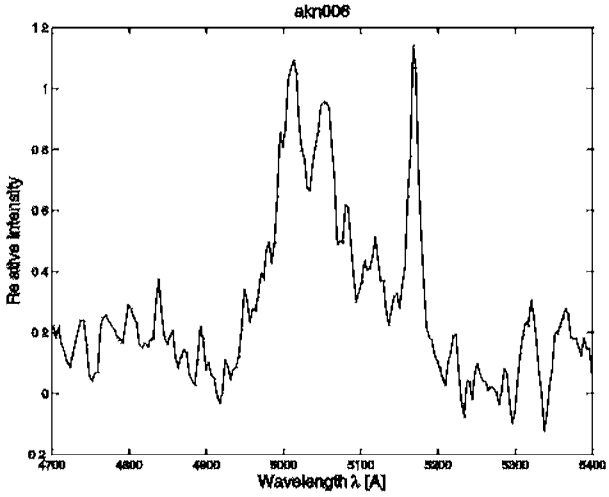
akn006
Relative Intensity
Wavelength λ [A]

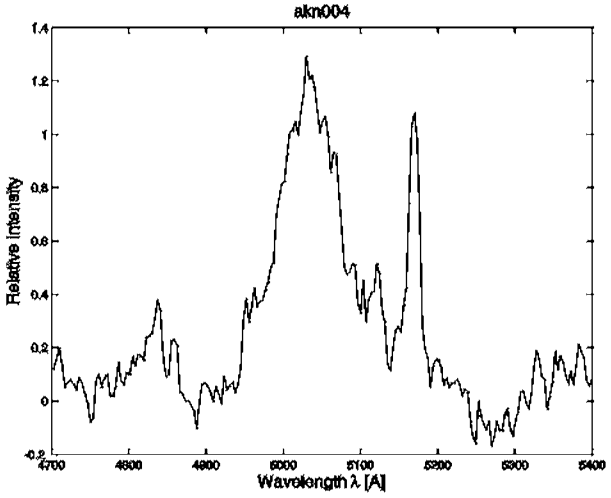
akn004
Relative Intensity
Wavelength λ [A]

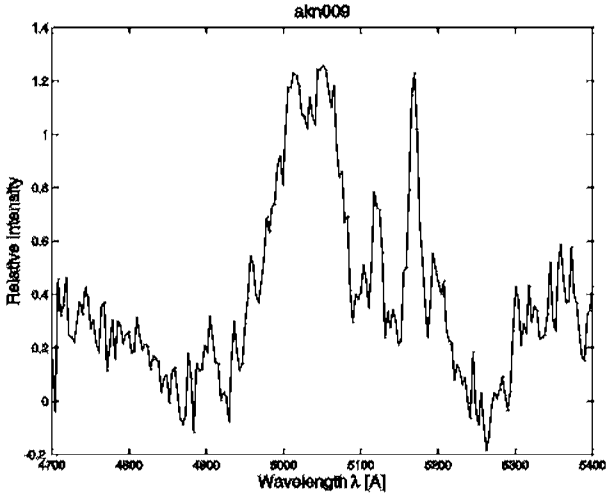
akn009
Relative Intensity
Wavelength λ [A]

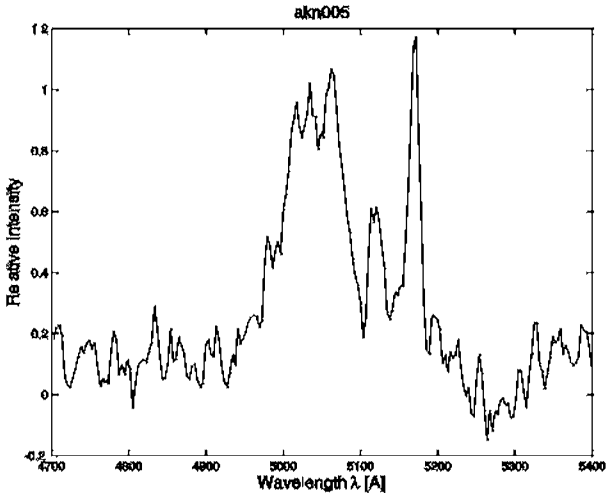
akn005
Relative Intensity
Wavelength λ [A]

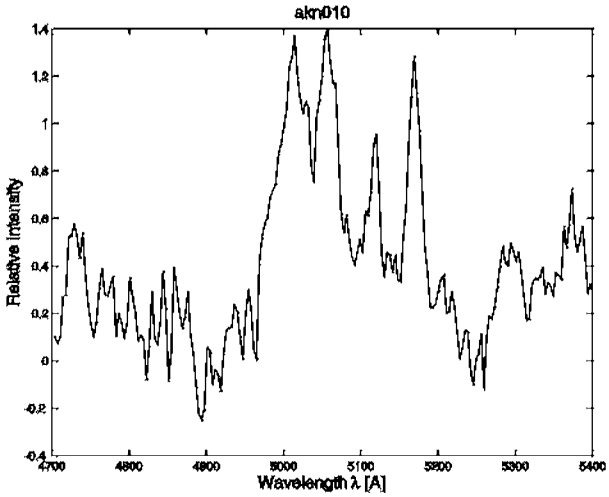
akn010
Relative Intensity
Wavelength λ [A]

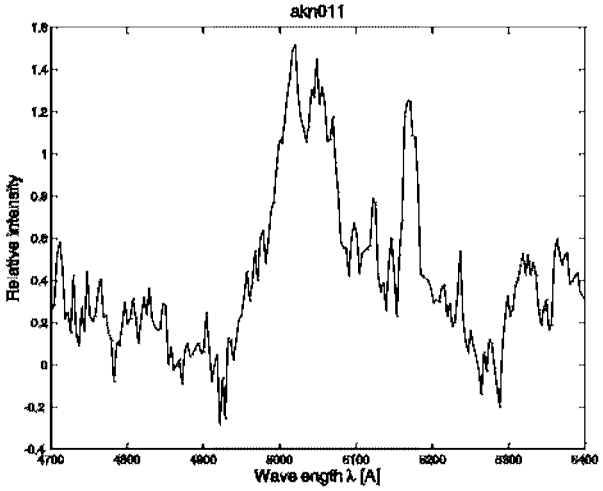
akn011
Relative Intensity
Wave ength λ [A]

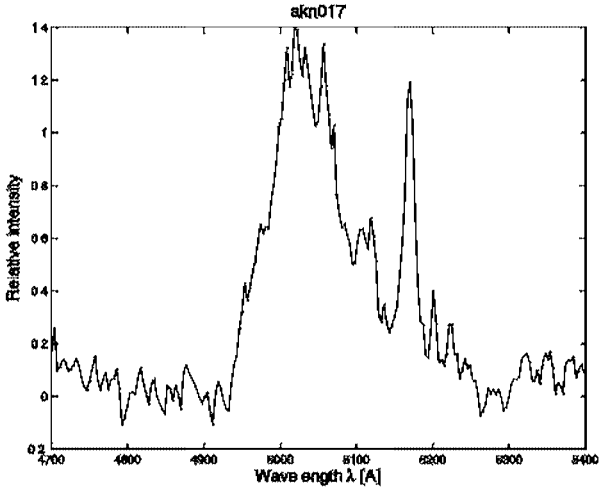
akn017
Relative Intensity
Wave ength λ [A]

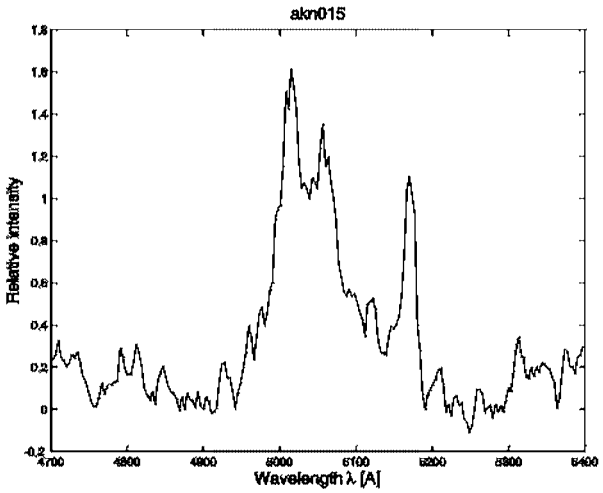
akn015
Relative Intensity
Wavelength λ [A]

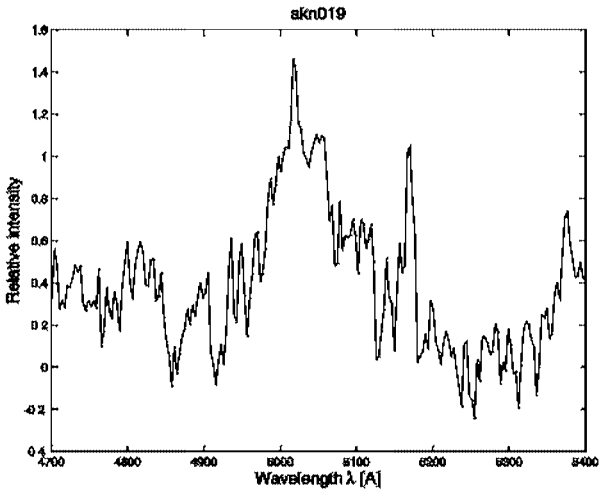
akn019
Relative Intensity
Wavelength λ [A]

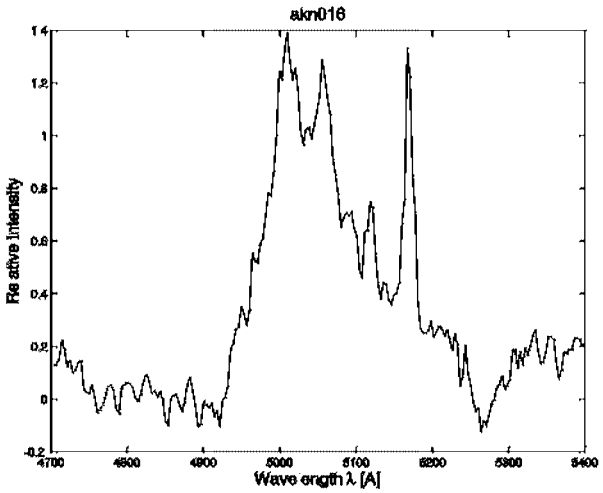
akn016
Relative Intensity
Wave ength λ [A]

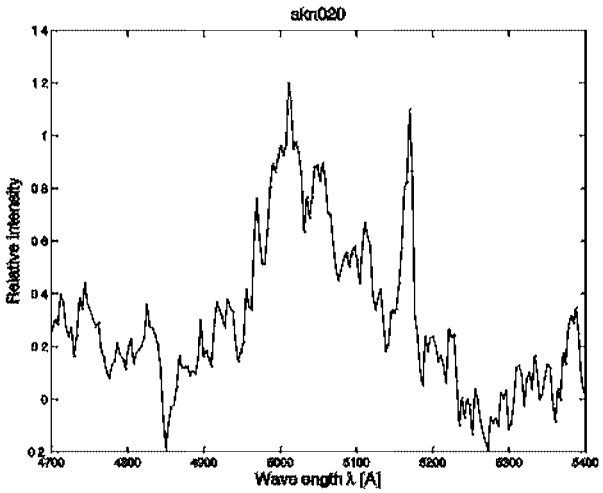
akn020
Relative Intensity
Wave ength λ [A]

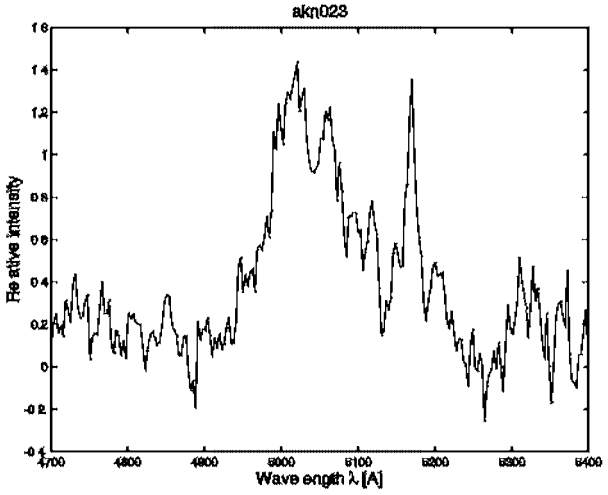
akn023
Relative Intensity
Wavelength λ [A]

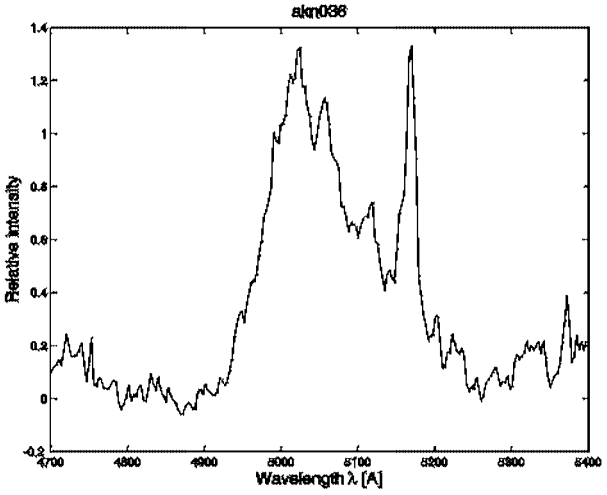
akn036
Relative Intensity
Wavelength λ [A]

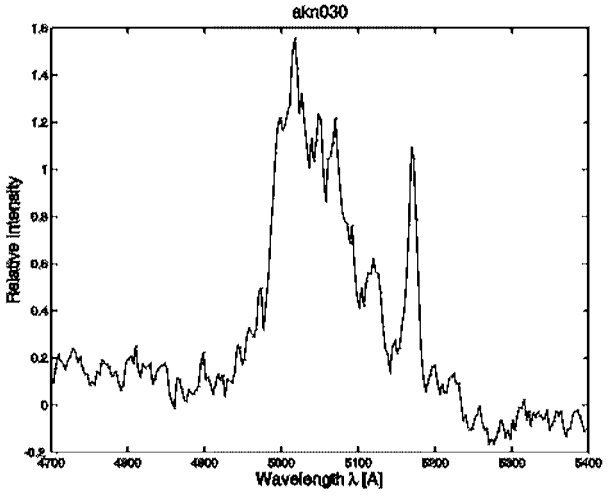
akn030
Relative Intensity
Wavelength λ [A]

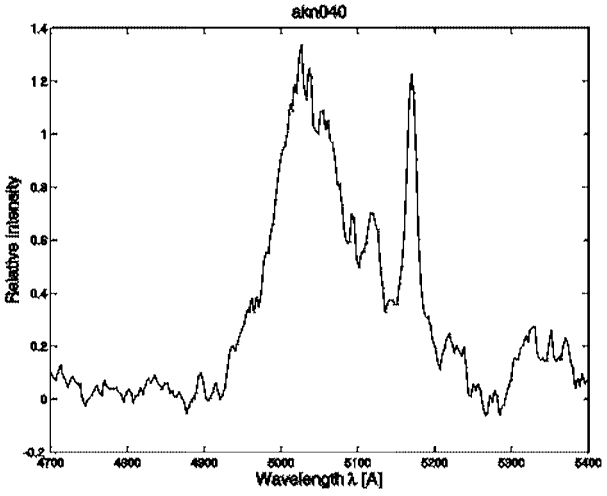
akn040
Relative Intensity
Wavelength λ [A]

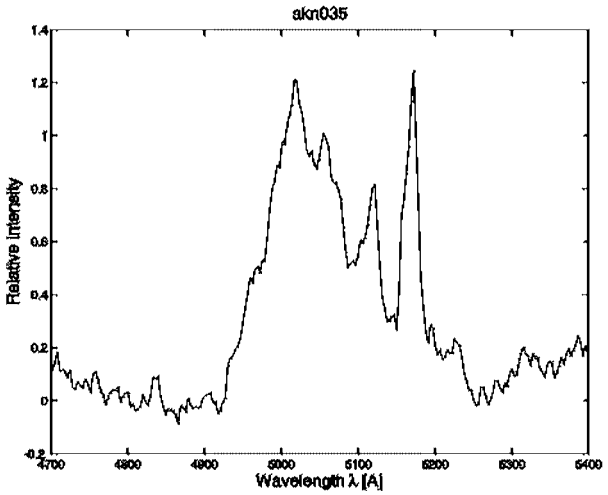
akn035
Relative Intensity
Wavelength λ [A]

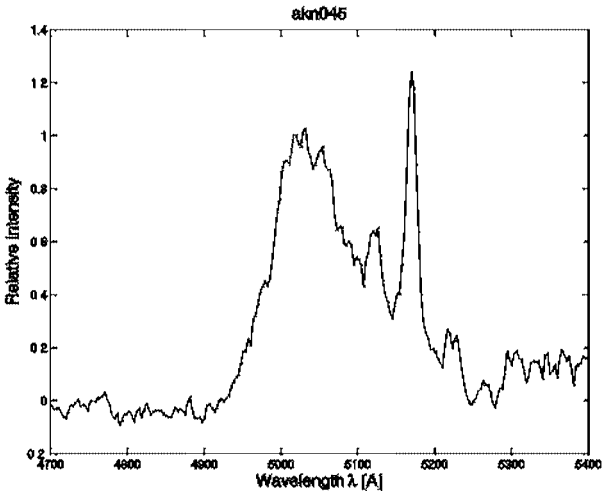
akn045
Relative Intensity
Wavelength λ [A]

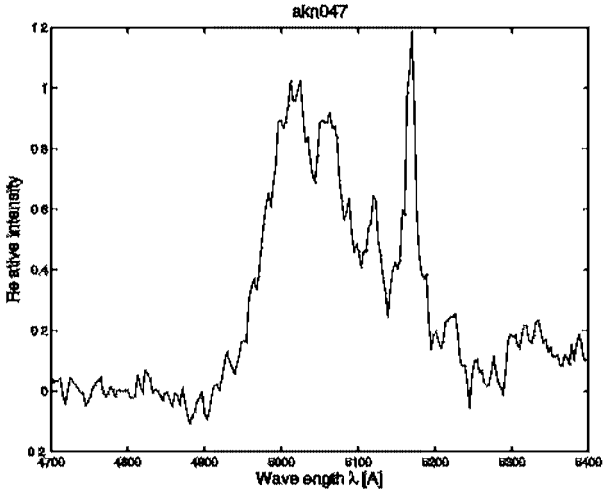
akn047
Relative Intensity
Wavelength λ [A]

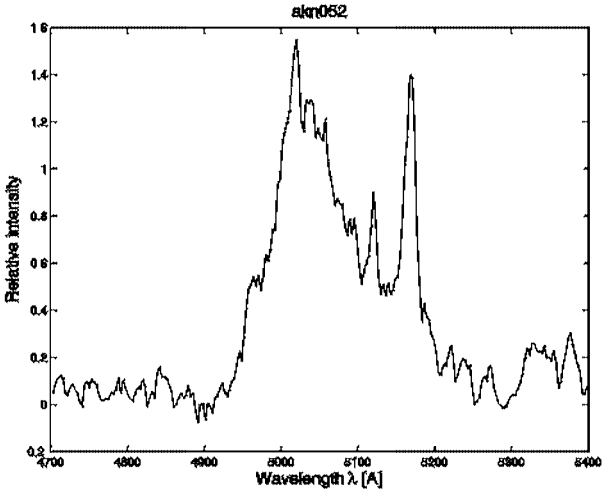
akn052
Relative Intensity
Wavelength λ [A]

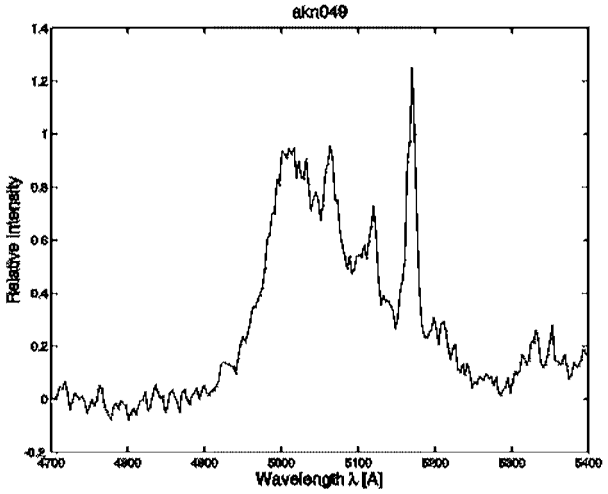
akn049
Relative Intensity
Wavelength λ [A]

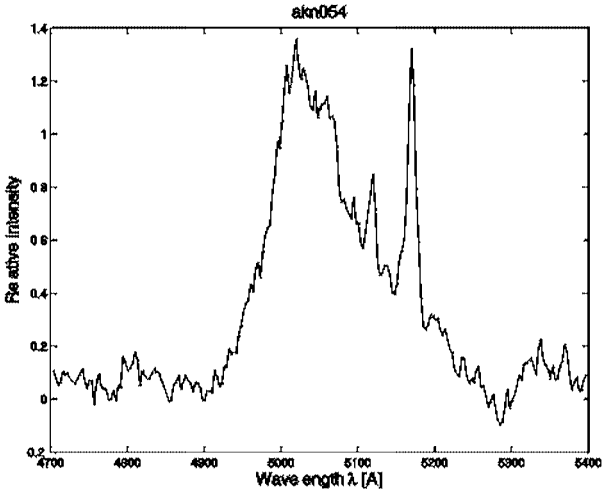
akn054
Relative Intensity
Wavelength λ [A]

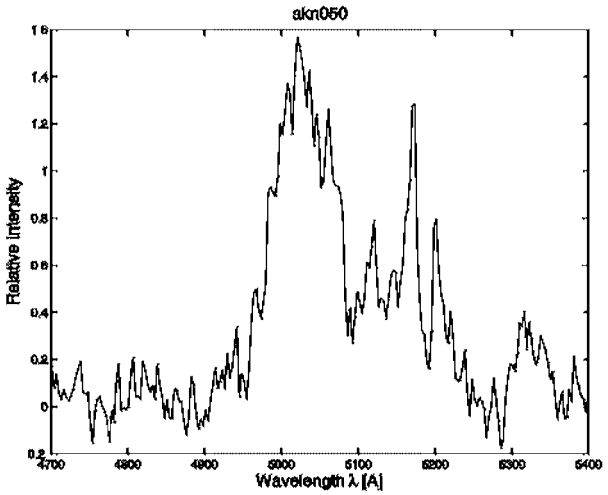
akn050
Relative Intensity
Wavelength λ [A]

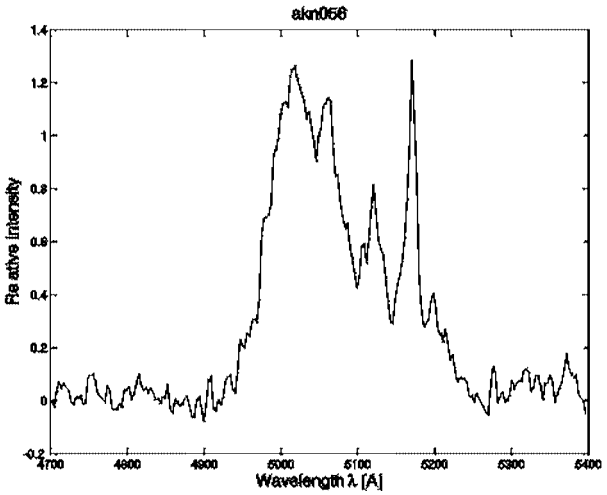
akn056
Relative Intensity
Wavelength λ [A]

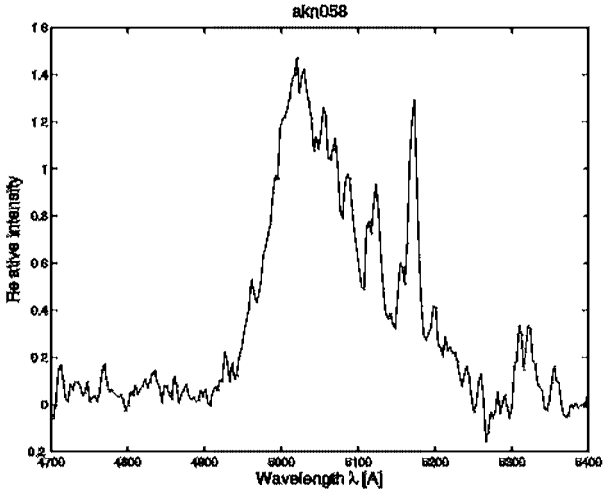
akn058
Relative intensity
Wavelength λ [A]

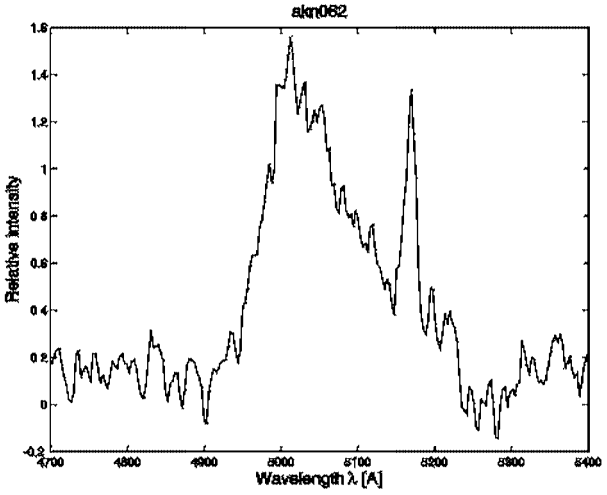
akn062
Relative intensity
Wavelength λ [A]

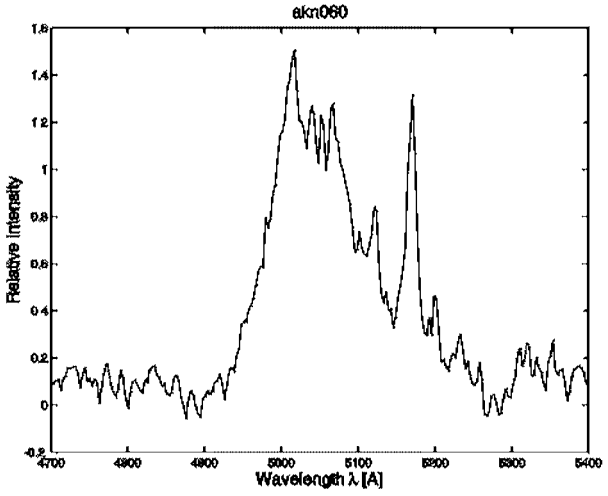
akn060
Relative intensity
Wavelength λ [A]

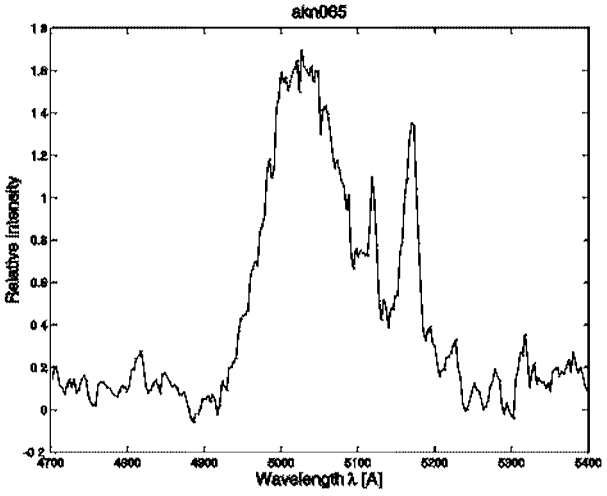
akn065
Relative intensity
Wavelength λ [A]

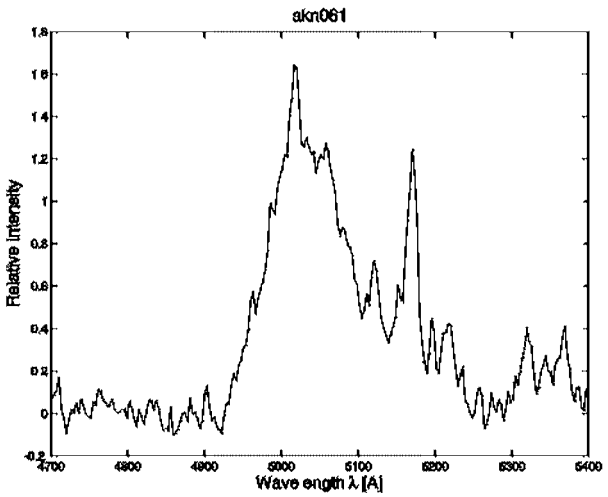
akn061
Relative intensity
Wave ength λ [A]

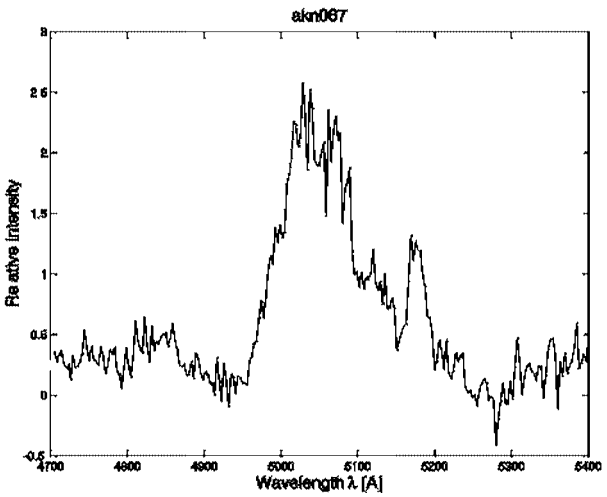
akn067
Relative intensity
Wavelength λ [A]

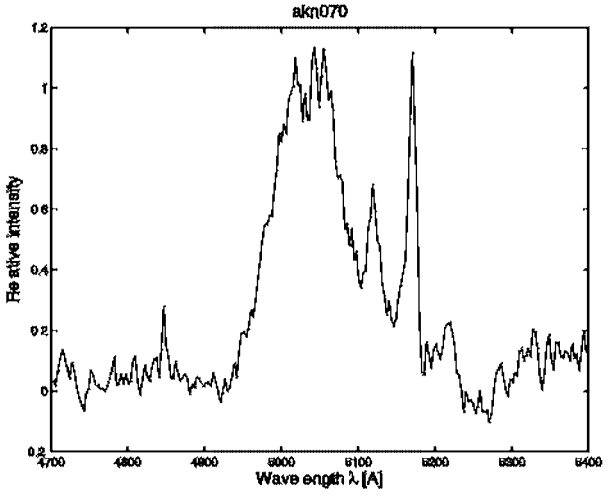
akn070
Relative intensity
Wavelength λ [A]

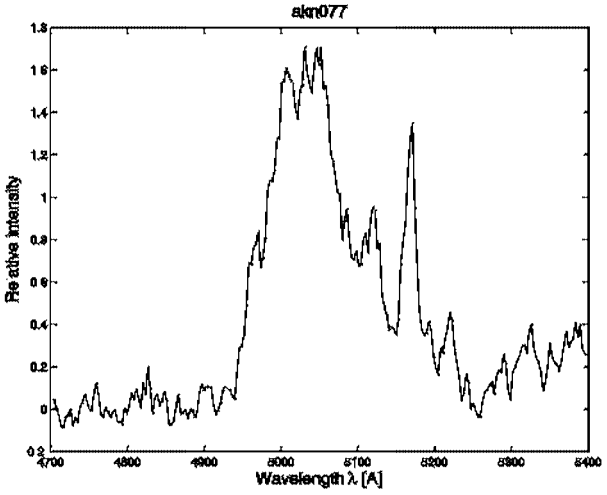
akn077
Relative intensity
Wavelength λ [A]

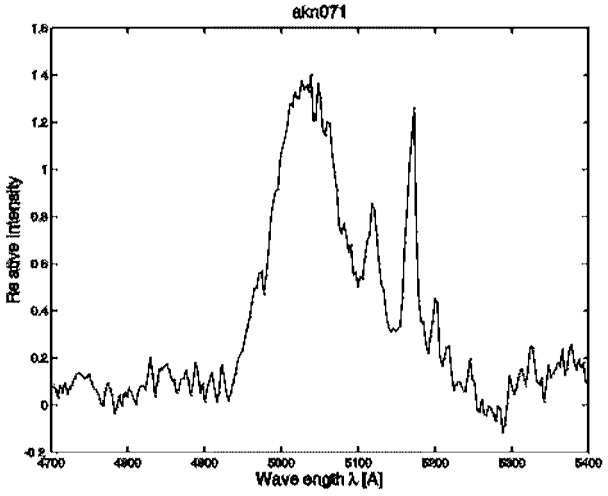
akn071
Relative intensity
Wavelength λ [A]

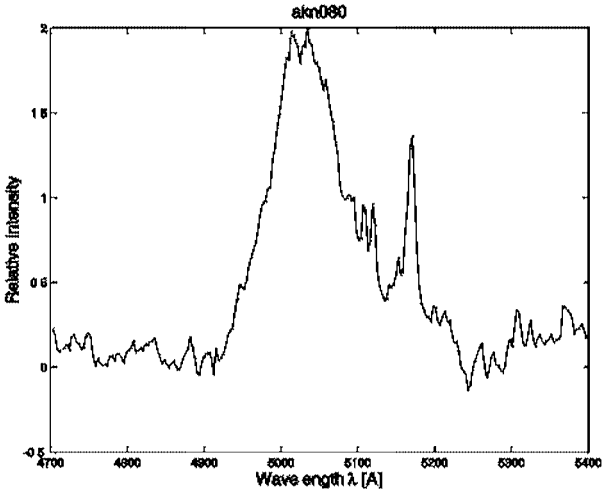
akn080
Relative intensity
Wavelength λ [A]

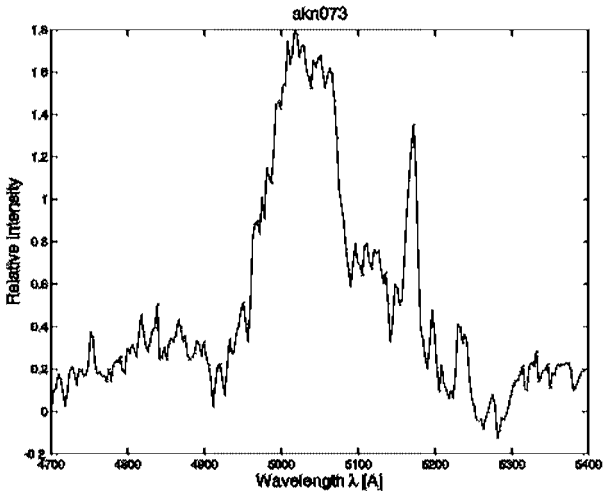
akn073
Relative intensity
Wavelength λ [A]

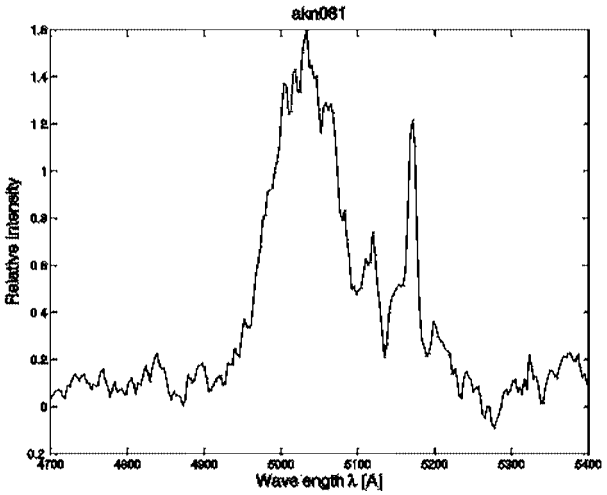
akn061
Relative intensity
Wavelength λ [A]

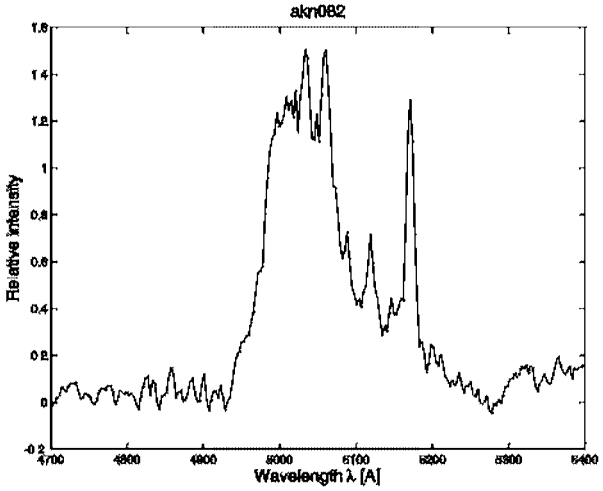
akn082
Relative Intensity
Wavelength λ [A]

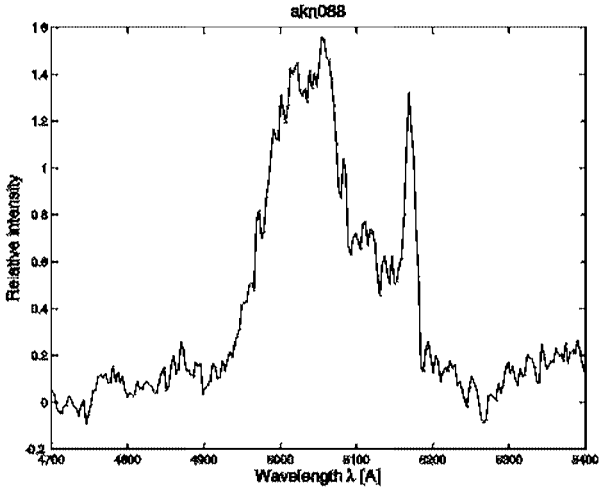
akn088
Relative Intensity
Wavelength λ [A]

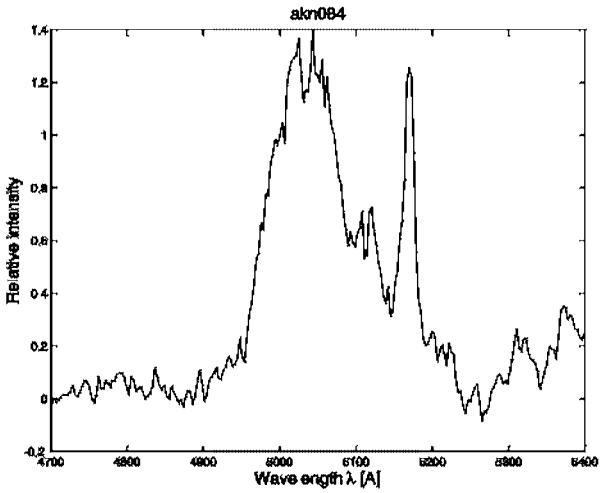
akn084
Relative Intensity
Wave ength λ [A]

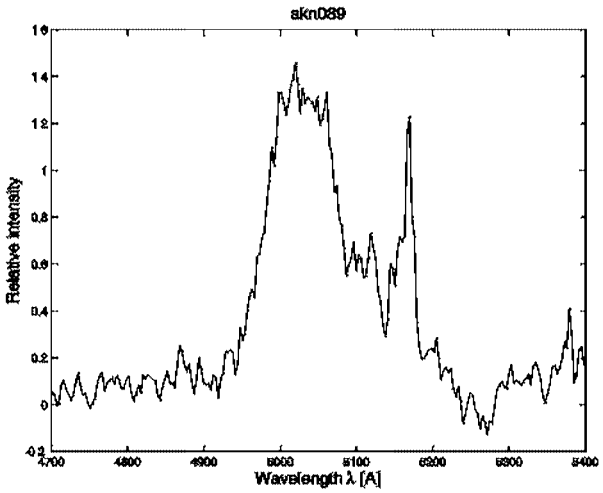
akn089
Relative Intensity
Wavelength λ [A]

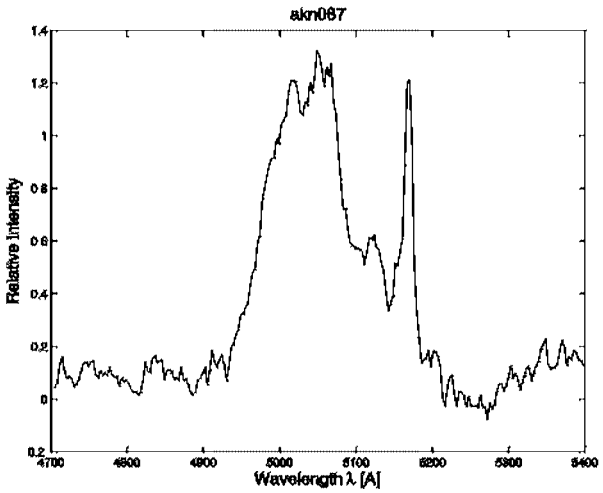
akn087
Relative Intensity
Wavelength λ [A]

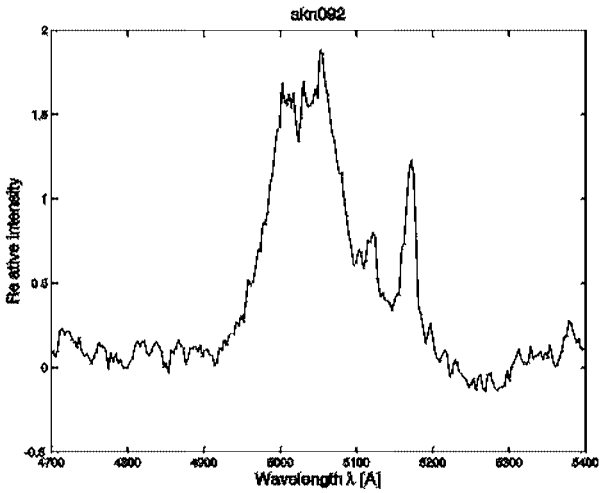
akn092
Relative Intensity
Wavelength λ [A]

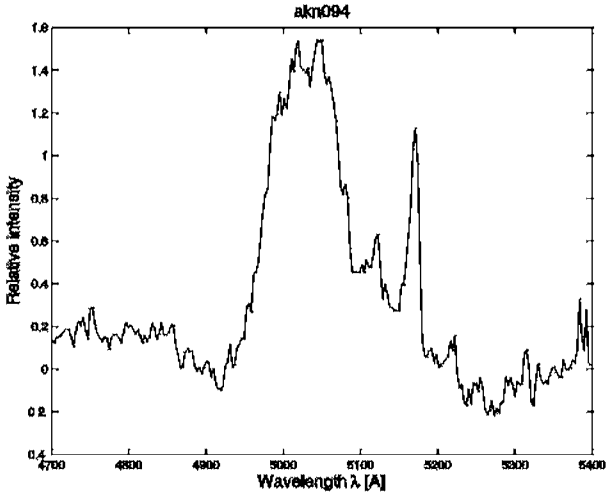
akn094
Relative Intensity
Wavelength λ [A]

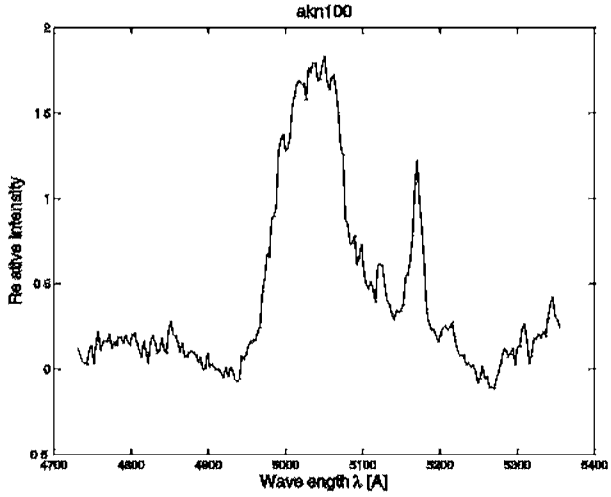
akn100
Relative Intensity
Wavelength λ [A]

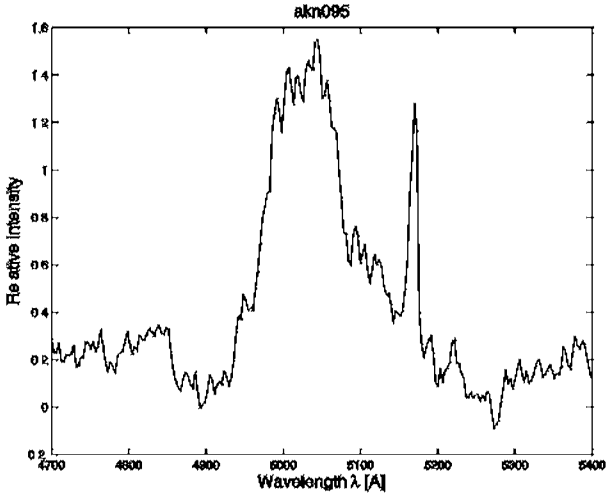
akn095
Relative Intensity
Wavelength λ [A]

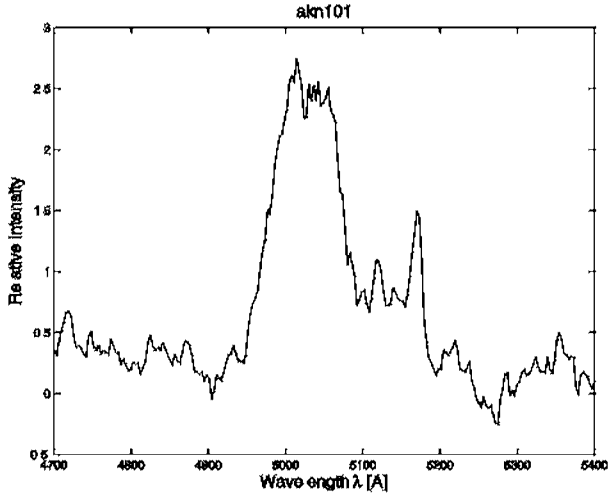
akn101
Relative Intensity
Wavelength λ [A]

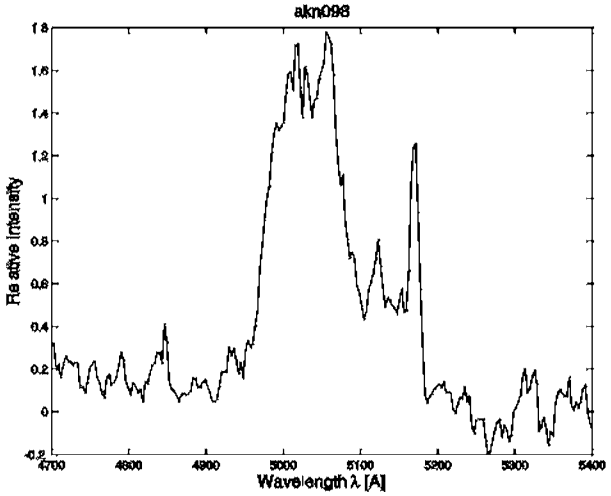
akn098
Relative Intensity
Wavelength λ [A]

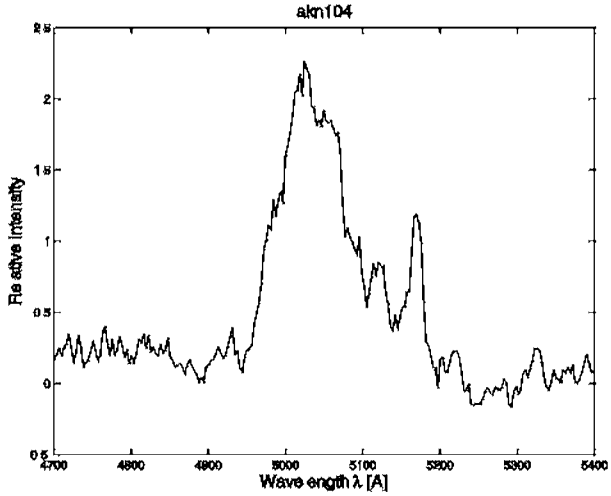
akn104
Relative Intensity
Wavelength λ [A]

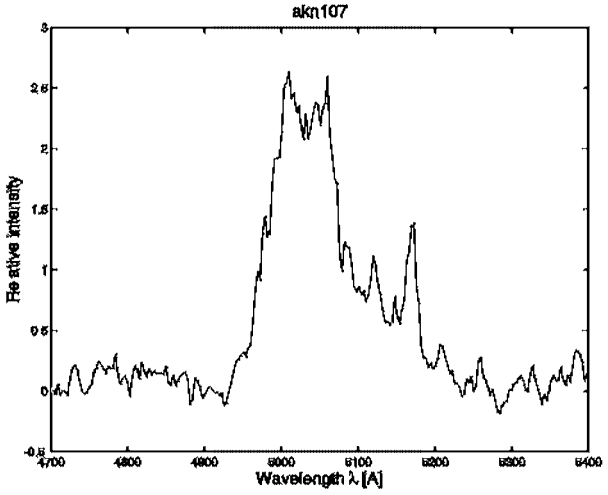
akn107
Relative Intensity
Wavelength λ [A]

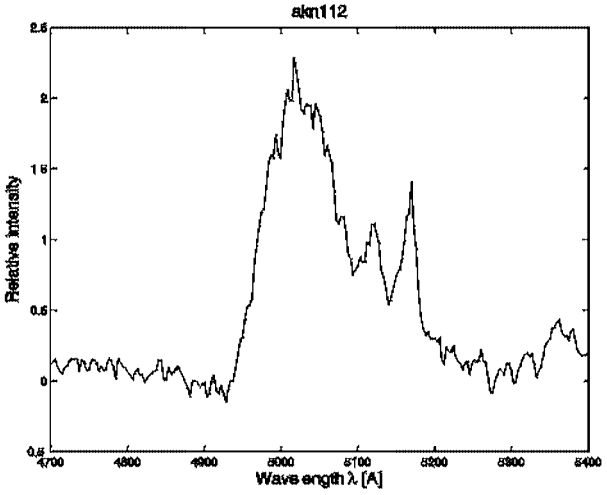
akn112
Relative Intensity
Wavelength λ [A]

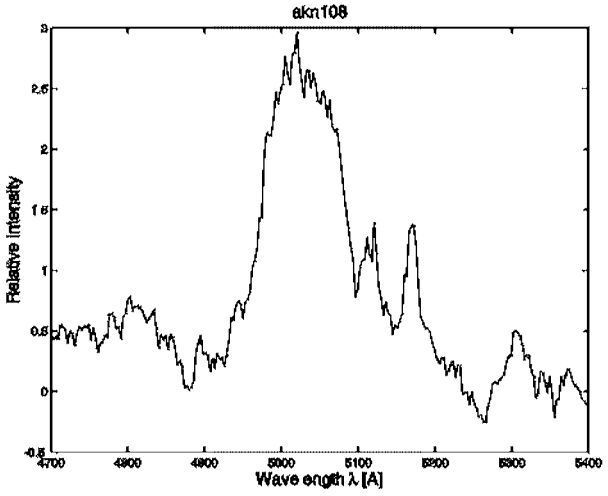
akn108
Relative Intensity
Wavelength λ [A]

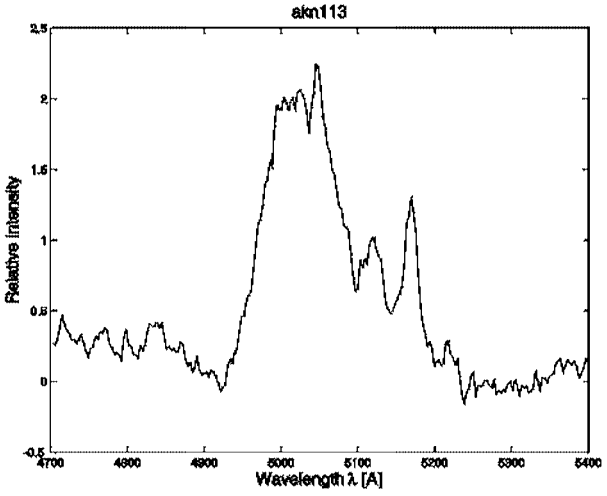
akn113
Relative Intensity
Wavelength λ [A]

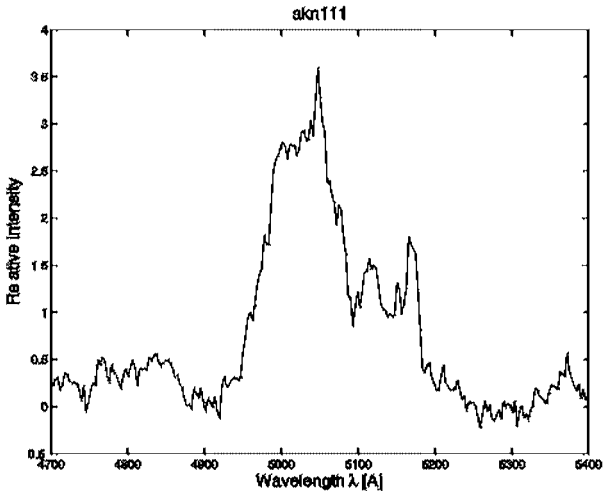
akn111
Relative Intensity
Wavelength λ [A]

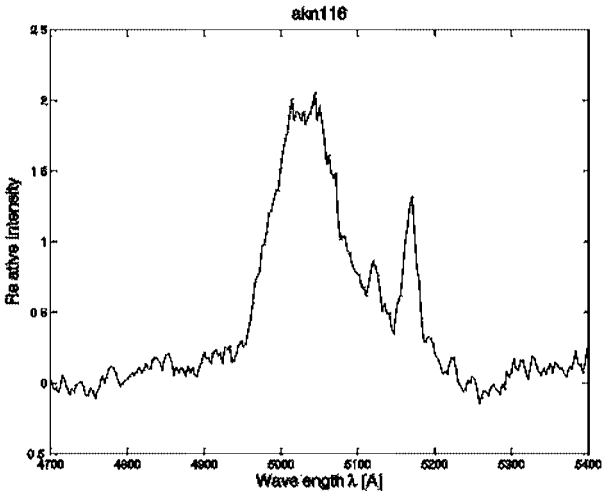
akn116
Relative Intensity
Wavelength λ [A]

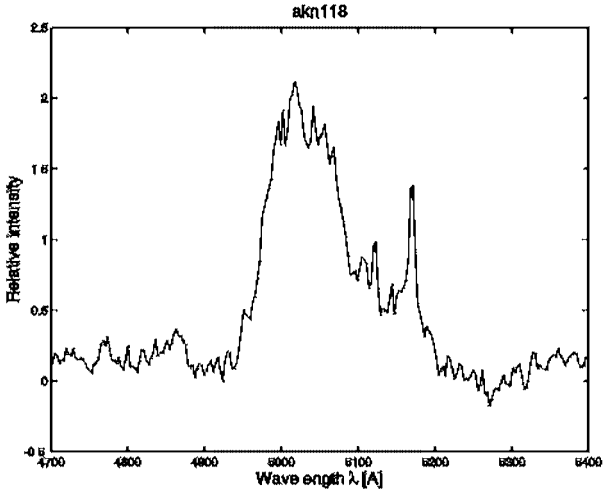
akn118
Relative intensity
Wave ength λ [A]

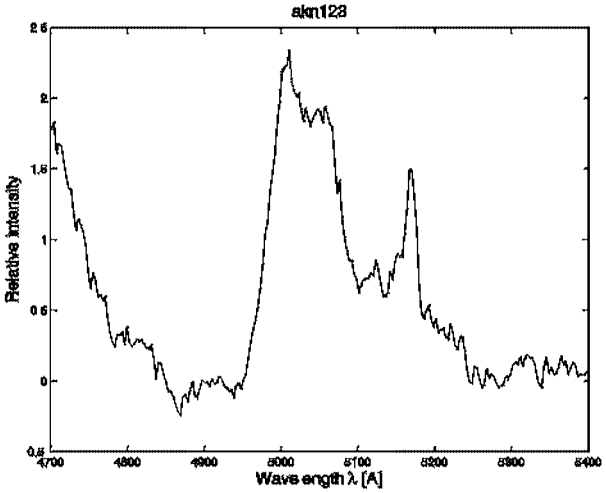
akn123
Relative intensity
Wave ength λ [A]

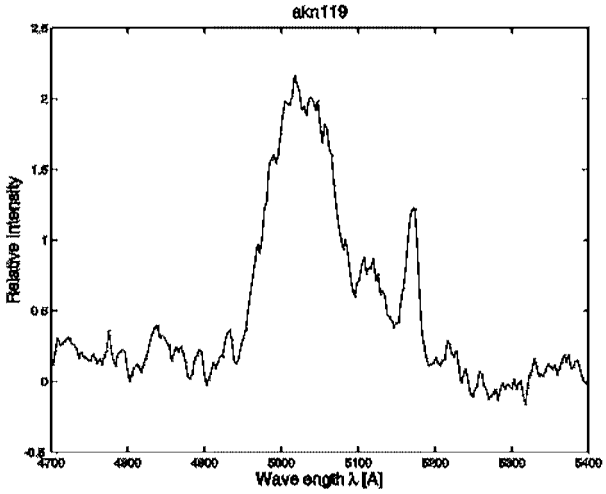
akn119
Relative intensity
Wave ength λ [A]

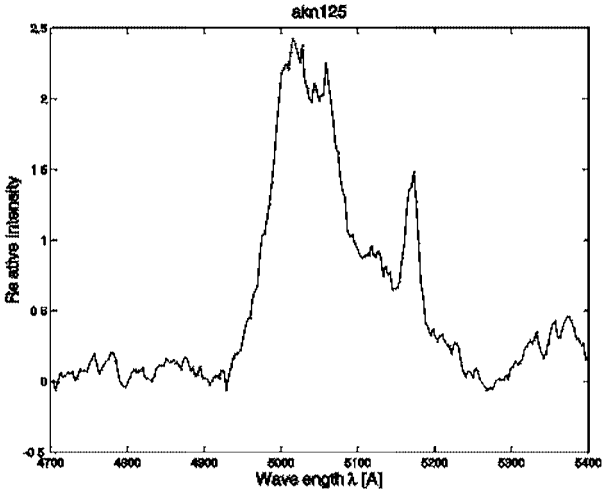
akn125
Relative intensity
Wave ength λ [A]

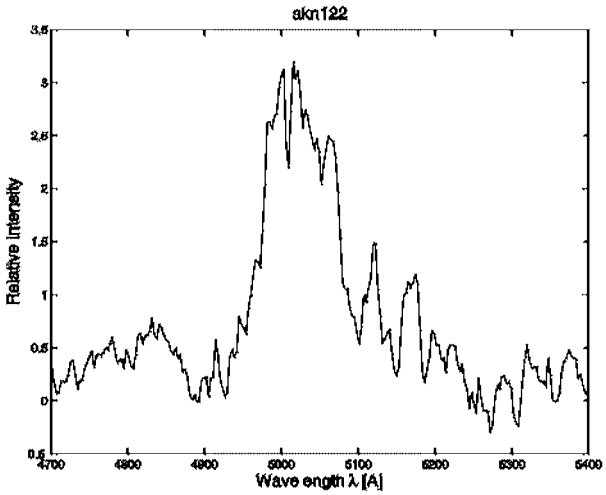
akn122
Relative intensity
Wave ength λ [A]

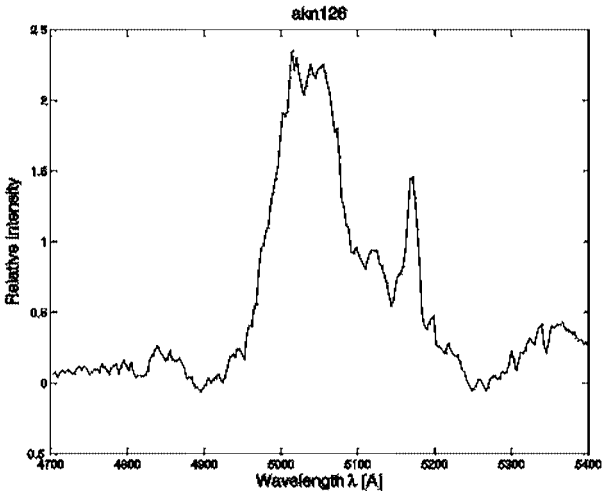
akn126
Relative intensity
Wavelength λ [A]

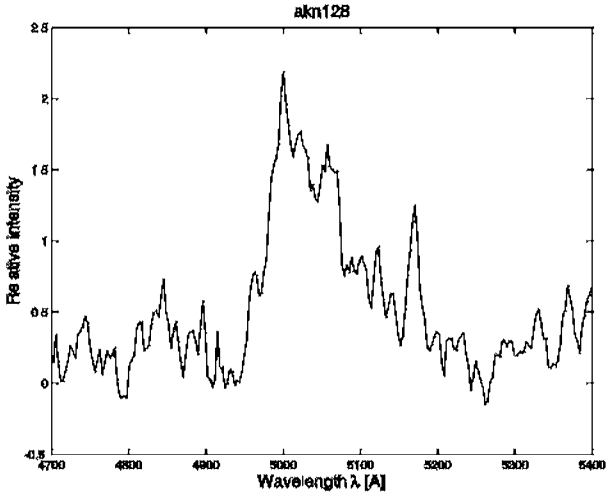
akn128
Relative Intensity
Wavelength λ [A]

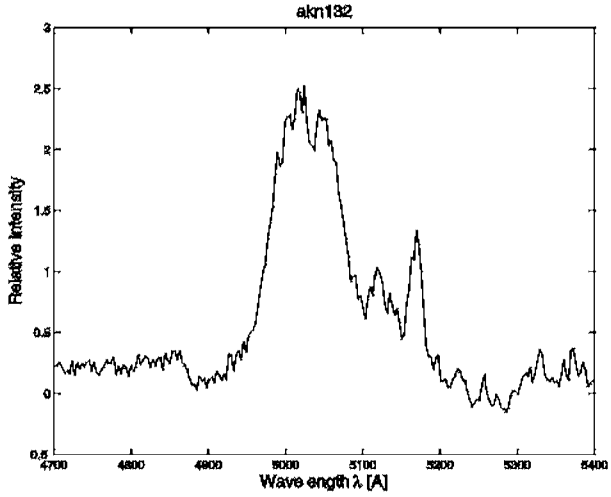
akn132
Relative Intensity
Wavelength λ [A]

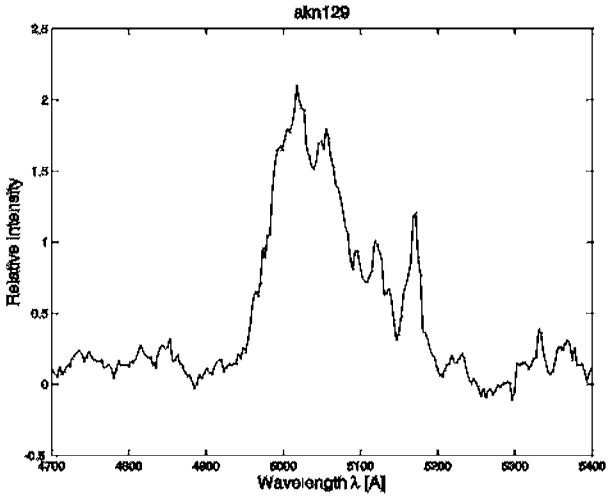
akn129
Relative Intensity
Wavelength λ [A]

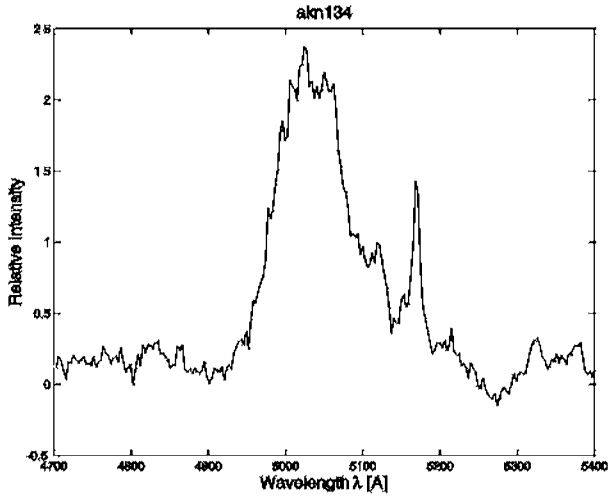
akn134
Relative Intensity
Wavelength λ [A]

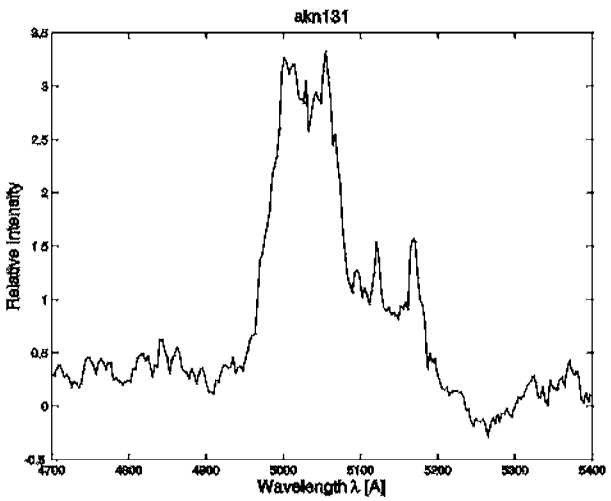
akn131
Relative Intensity
Wavelength λ [A]

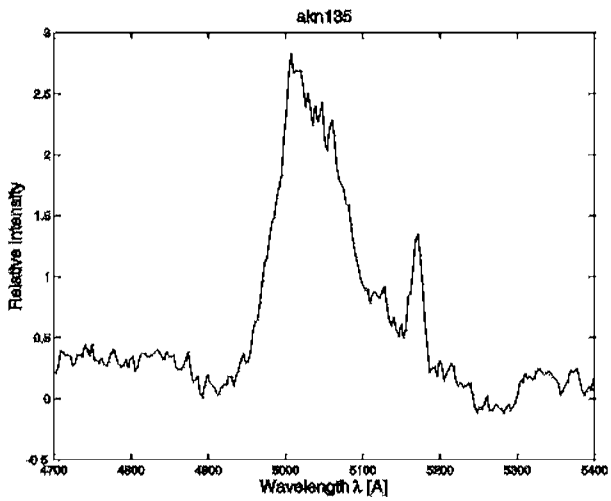
akn135
Relative Intensity
Wavelength λ [A]

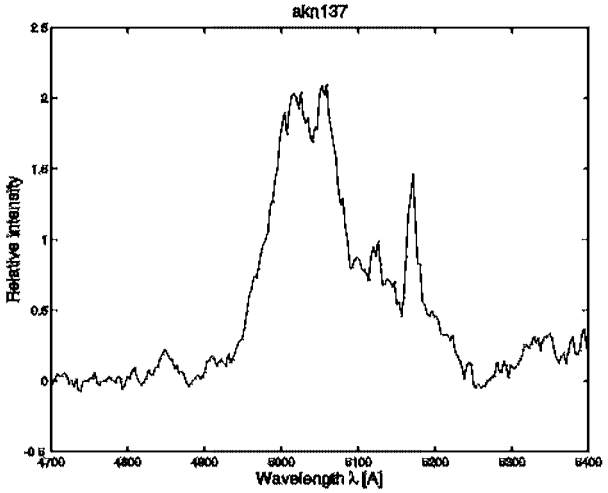
akn137
Relative intensity
Wavelength λ [A]

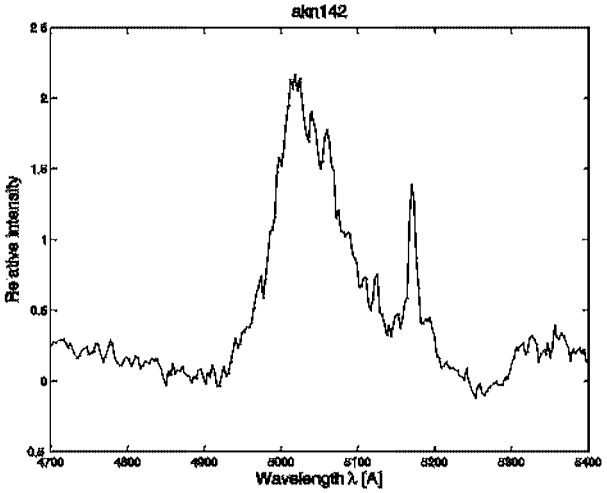
akn142
Relative intensity
Wavelength λ [A]

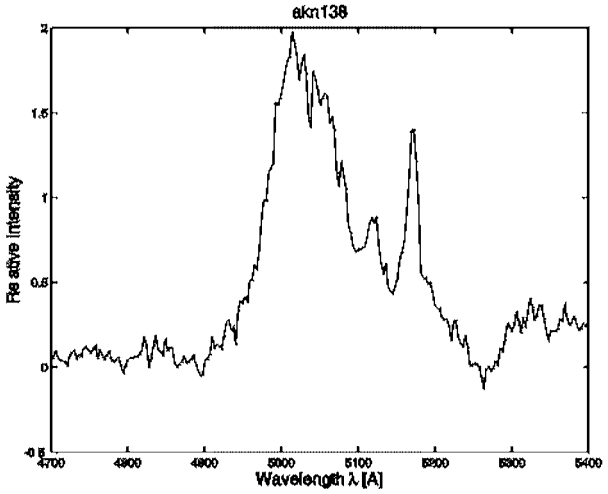
akn138
Relative intensity
Wavelength λ [A]

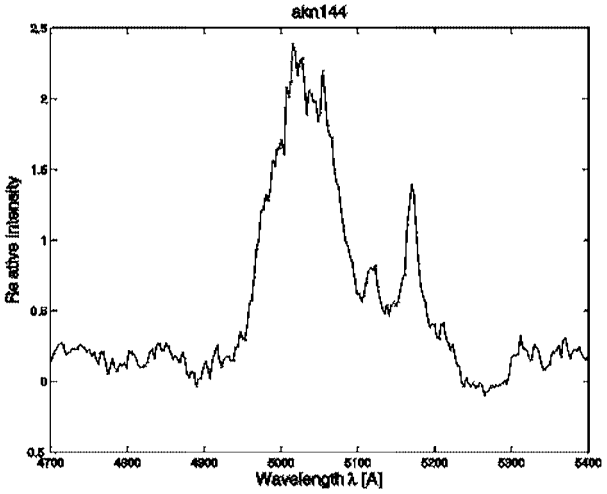
akn144
Relative intensity
Wavelength λ [A]

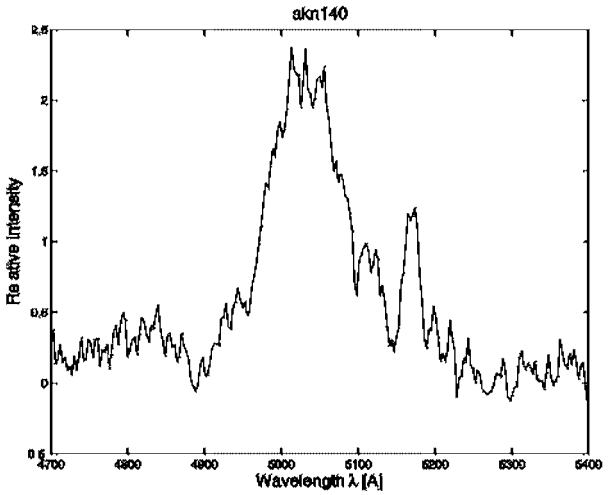
akn140
Relative intensity
Wavelength λ [A]

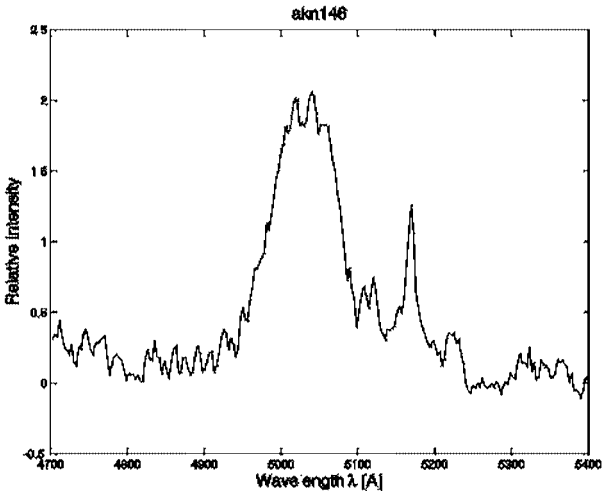
akn146
Relative intensity
Wavelength λ [A]

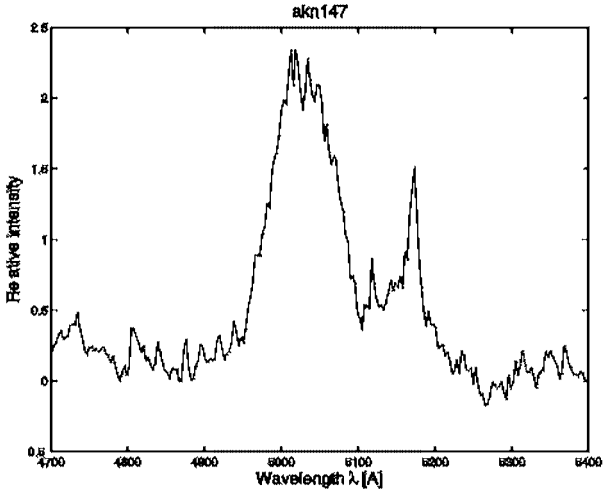
akn147
Relative intensity
Wavelength λ [A]

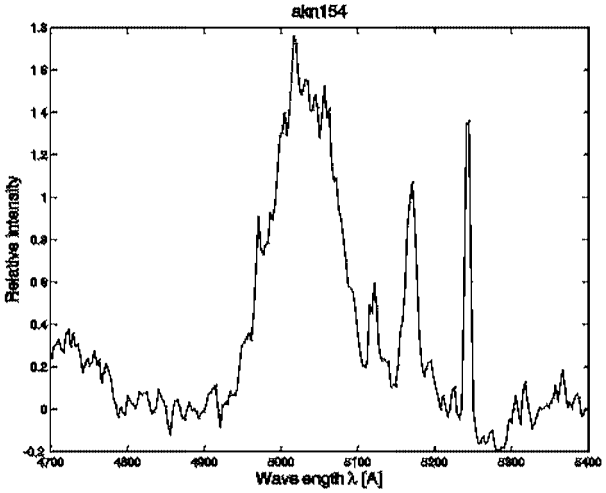
akn154
Relative intensity
Wavelength λ [A]

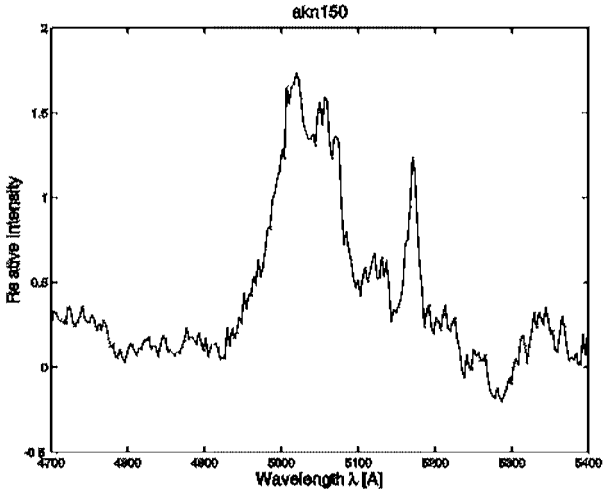
akn150
Relative intensity
Wavelength λ [A]

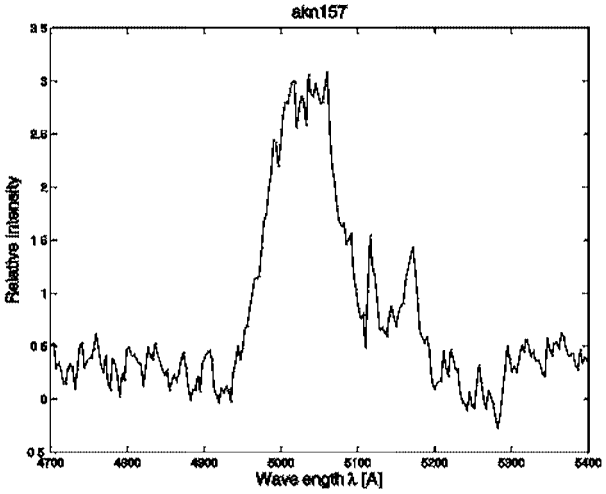
akn157
Relative intensity
Wavelength λ [A]

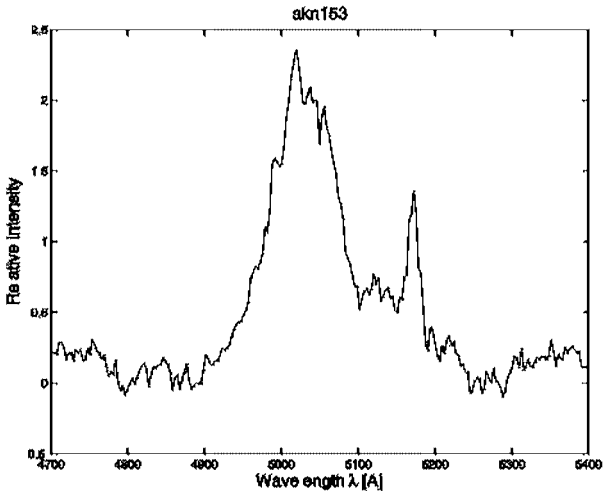
akn153
Relative intensity
Wavelength λ [A]

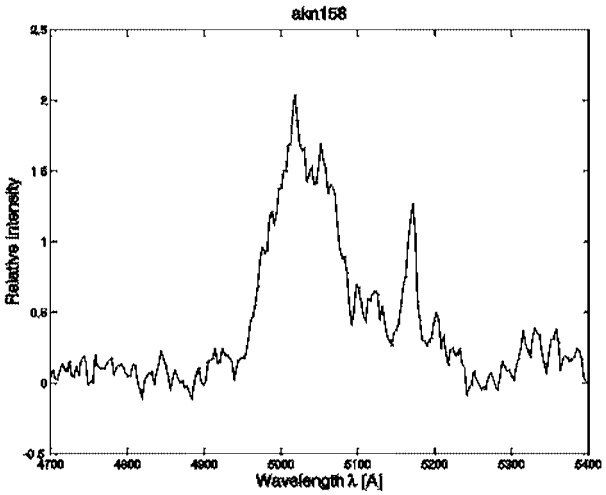
akn158
Relative intensity
Wavelength λ [A]

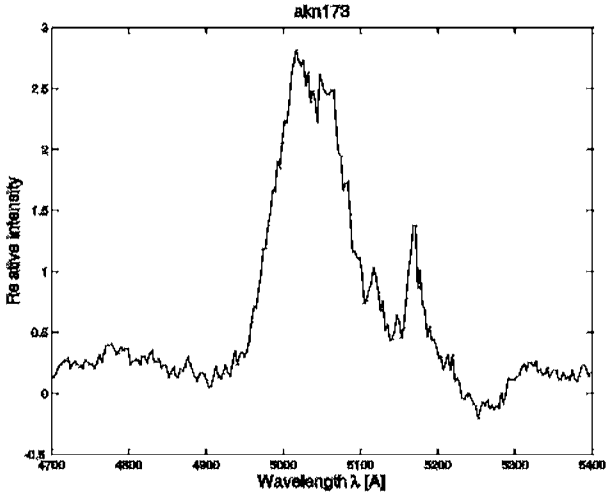
akn173
Relative Intensity
Wavelength λ [A]

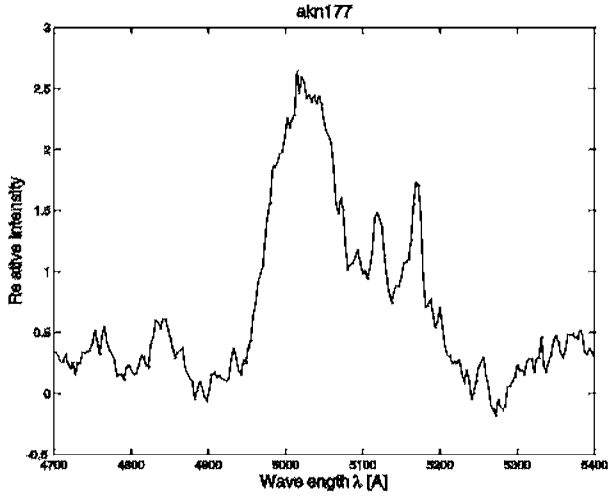
akn177
Relative Intensity
Wavelength λ [A]

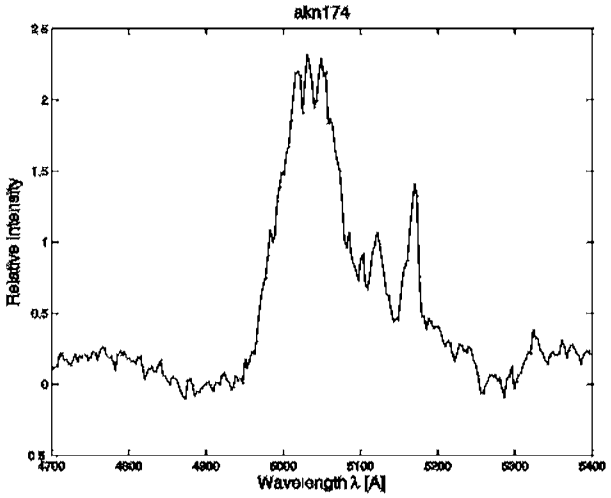
akn174
Relative Intensity
Wavelength λ [A]

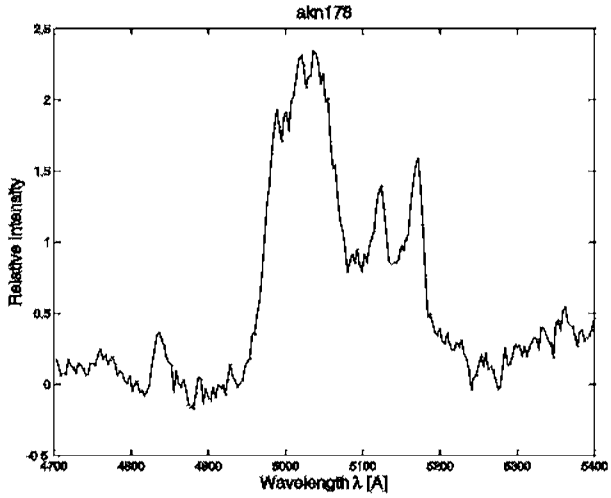
akn178
Relative Intensity
Wavelength λ [A]

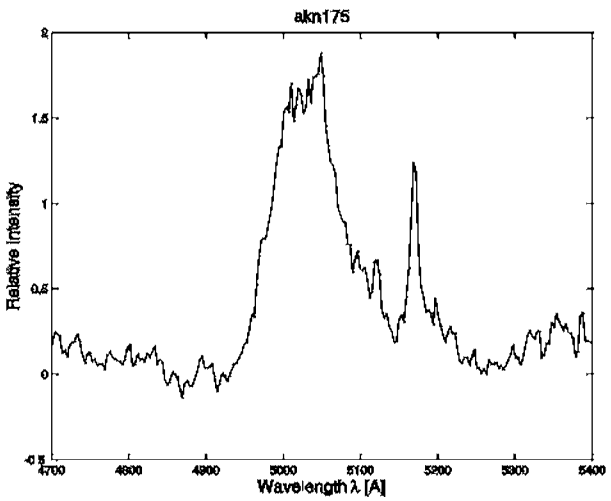
akn175
Relative Intensity
Wavelength λ [A]

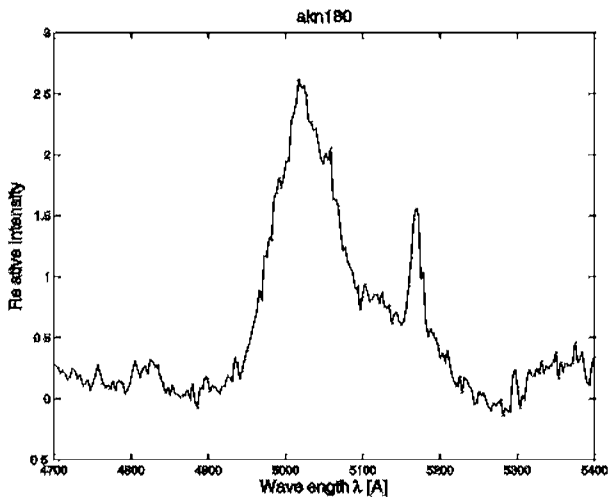
akn180
Relative Intensity
Wavelength λ [A]

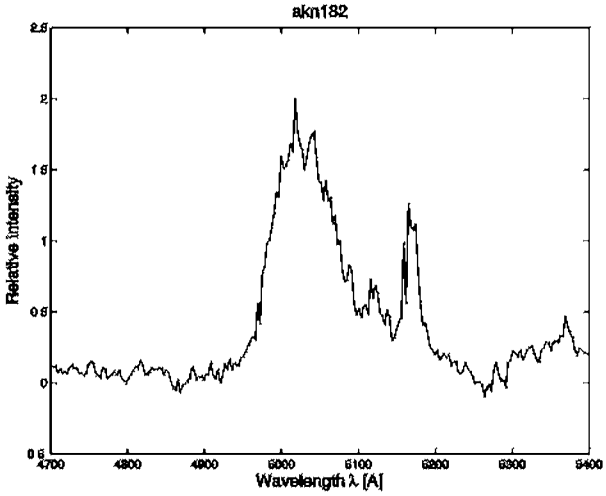
akn182
Relative Intensity
Wavelength λ [A]

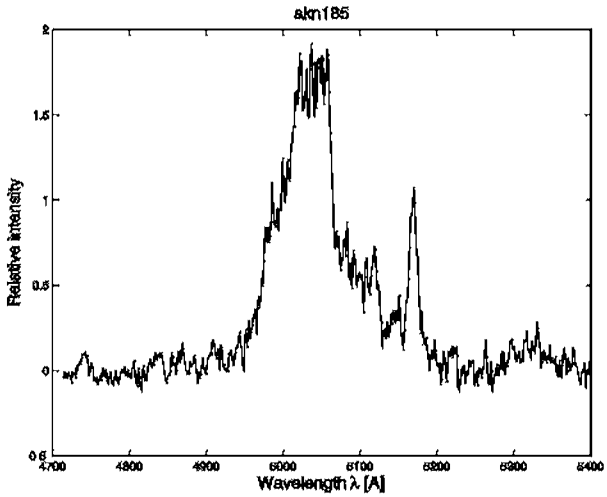
akn185
Relative Intensity
Wavelength λ [A]

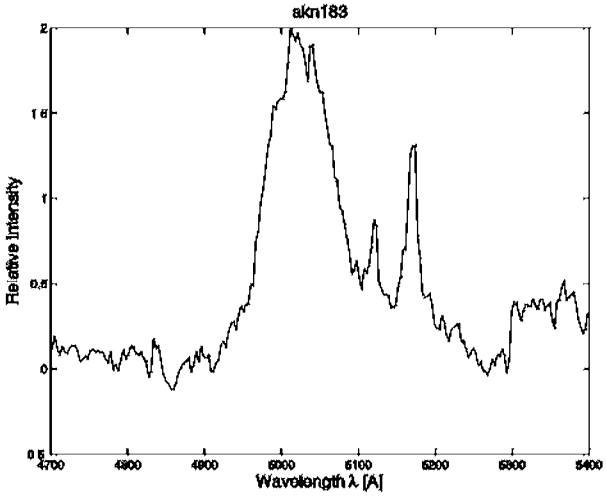
akn183
Relative Intensity
Wavelength λ [A]

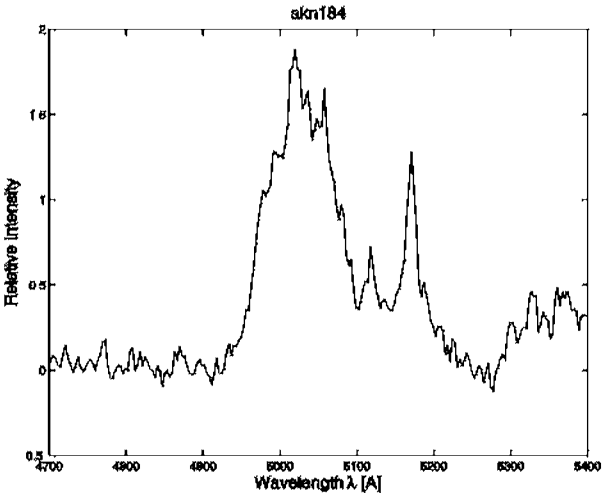
akn184
Relative Intensity
Wavelength λ [A]

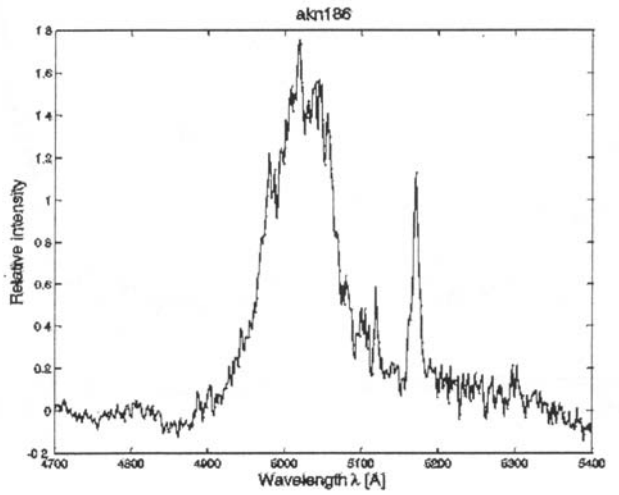
akn186
Relative intensity
Wavelength λ [Å]

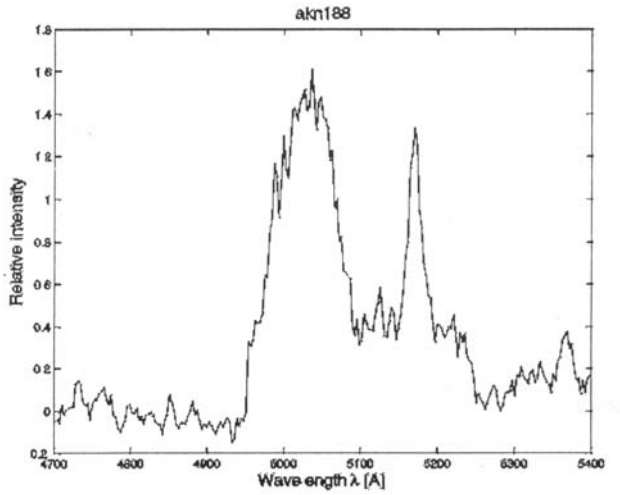
akn188
Relative intensity
Wave ength λ [Å]

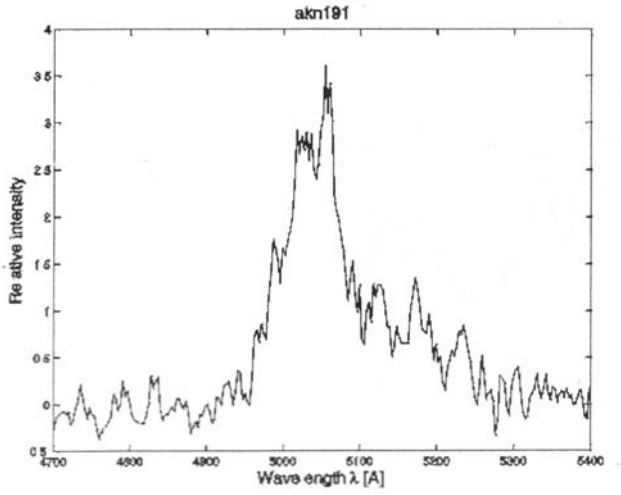
akn191
Re ative intensity
Wave ength λ [Å]

ОБЛИК H_β ЛИНИЈЕ КОД Акн120

Н. Станић, Л. Ч. Поповић, А. Кубичела и Е. Бон

Астрономска опсерваторија, Волгина 7, 11160 Београд–74, Југославија

УДК 52–355.3/524.7–82
Оригинални научни рад

Представљено је 96 спектара H_β линије код активне галаксије Акн 120, посматраних са Кримске астрофизичке опсерваторије у периоду од 1977. до 1990. (Appendix 1). H_β линија се може разложити на три широке и једну уску гаусову функцију код свих посматраних спектара. Централна компонента и линије гвожђа у црвеном крилу H_β линије доводе до промена профила линије. Из профила се може закључити да он настаје у три региона у широколинијској области и једног у усколинијској области. Дискутована је промена у облику профила H_β линије.